Modeling and Velocity-Field Control of Autonomous Excavator with Main Control Valve ⋆

Kwangmin Kim [a], Minji Kim [a], Dongmok Kim [b], Dongjun Lee [a,*]

[a] *Department of Mechanical & Aerospace Engineering and IAMD, Seoul National University, Seoul 08826, Republic of Korea*

[b] *Global R&D Center, Doosan Infracore Co., Ltd., Incheon 22502, Republic of Korea*

Abstract

We propose a novel modeling and control framework for the autonomous excavator with main control valve (MCV), which distributes fluid from pumps to hydraulic actuators with the number of the pumps less than that of the actuators and whose internal hydraulic circuitry switches depending on operating conditions and internal pressures. We first derive the mathematical model of the MCV, including the switching components and supply pump flow constraint. We then design a novel velocity-field control for the bucket position/orientation, which, by relying on a constrained-optimization formulation, can adjust the velocity-field following speed reflecting the physical constraints imposed by the MCV in such a way that the bucket fully follows the desired velocity-field when the constraints are inactive or still preserves the desired direction (or automatic stopping) while slowing down when the constraints become active (e.g. flow saturation). We further show that this optimization can be reduced to simple real-time solvable formulation with its solution existence/optimality (or suboptimality) guaranteed. Simulation is also performed to verify the theory by using a detailed Simulink/Sim-Hydraulics model.

Key words: Autonomous excavator, constrained optimization, hydraulic actuation, main control valve (MCV), velocity-field control

1 Introduction

With the advance of sensor and actuator hardwares, control and perception algorithms, and information technologies, the field of construction has increasingly been heading toward automation [5, 10, 12, 13, 19, 35]. This automated construction is deemed to bring substantial market competitiveness by allowing for operations impossible with human operators involved due to safety or occupational health concerns, while also significantly enhancing operation efficiency, fuel economy and system reliability [5,10,12,13,19,35]. Central to most of the construction operations is excavators, and their full or partial automation is thought to be crucial for the construction automation [1, 7–9, 11, 17, 18, 20, 21, 24, 25, 28, 33].

The key challenging aspect for automatic control of these construction excavators is their adoption of hydraulic actuation, which boasts higher power-to-size ratio and robustness as compared to, e.g., electrical motors. This problem of hydraulic excavator control has been the subject of active investigation with many strong results proposed (e.g. motion control [1, 7, 25], force control [17, 20, 33], interaction control [24]). These (and other) results for the excavator control, yet, typically assume each degree-of-freedom (DOF) of the excavator (i.e. bucket, arm, boom) be controlled individually and separately by its own hydraulic system (i.e. flow pump, valve, cylinder). See also [4,6,16,27,32] for the results of this single-DOF hydraulic system control for other application domains.

Most of the industrial construction excavators, however, are equipped with fewer number of pumps than the hydraulic cylinders to reduce manufacturing and maintenance cost while also improving fuel efficiency via down-

⋆ Research supported by the Basic Science Research Program (2015R1A2A1A15055616) through the National Research Foundation (NRF) funded by the Ministry of Science, ICT & Future Planning (MSIP), Korea; the Industrial Strategic Technology Development Program (10060070) funded by the Ministry of Trade, Industry & Energy (MOTIE), Korea; and Doosan Infracore BK21 Plus Support Program. This paper was not presented at any IFAC meeting.

* Corresponding author.

Email addresses: kkm0313@snu.ac.kr (Kwangmin Kim), minji8151@snu.ac.kr (Minji Kim), dongmok.kim@doosan.com (Dongmok Kim), djlee@snu.ac.kr (Dongjun Lee).

Fig. 1. Main control valve (MCV) of an industrial excavator, connecting less number of pumps to more number of hydraulic cylinders for cost effectiveness, reliability, energy efficiency and maintenance.

sizing. To actuate hydraulic cylinders with fewer supply pumps, the component, so called *main control valve* (MCV - see Fig. 1) is typically implemented in the industrial excavators, which routes the fluid from the pumps to all the valves and cylinders with its internal hydraulic circuitry also switching to adjust fluid distribution among the cylinders depending on the excavation tasks. This MCV then substantially complicates the modeling and control design problem of industrial excavator systems as compared to the case of single-DOF hydraulic systems (e.g. [1, 4, 6, 7, 16, 17, 20, 24, 25, 27, 32, 33]), since all the hydraulic components are now coupled with each other via this MCV with the internal configuration of the MCV possibly switching, which is triggered purely mechanically by the pressure/flow state of the MCV circuitry, thus, can be neither set nor predicted *a priori*. This complexity is even further exacerbated by that the flow supply of each pump is limited and also affected by the state of this MCV circuitry as well [2, 15].

In contrast to the abundance of results for the single-DOF hydraulic excavators and systems (e.g. [1,4,6,7,16, 17,20,24,25,27,32,33]), that with the MCV included are very rare, and, to our knowledge, only the result of [11] presents a model-based approach for the excavator control with the MCV, whose control objective yet is limited only to the straight line following, with no consideration on the pump flow supply limitation and spool actuation limits. Furthermore, the result in [11] relies on a piecewise-linear approximation of the nonlinear plant model, thus, not capable to adequately capture the important phenomenon of the hydraulic circuitry switching of the MCV. Other results for the excavator control with the MCV are [8, 21, 28], which are however not model-based and instead adopt learning-based approaches, thereby, avoiding the necessity to deal with the complexity stemming from the MCV as attained in this paper.

In this paper, we propose a novel model-based automatic control framework for this industrial excavator with MCV. For this, instead of fully-electrified MCVs, we choose the conventional (fully-mechanical) MCV with only its spool valves actuating the excavation cylinders electrically-controlled, since: 1) its implementation in industrial excavators is easier, since these spool valves are already mechanically connected to the joystick, which can be more conveniently replaced by electrical components than the full electrification of MCV; 2) its cost of hardware modification and control development are more affordable than those of full-electrification of MCV, which would require substantial redesign of MCV to embed those extra electrical valves in it and high cost of control development for all those electrical actuations; and 3) its analysis technique can easily be applied for the fully-electrified MCV, since, with more valves now controlled, the complexity of MCV behavior (e.g. purely mechanically-induced configuration switching) can be reduced. We do not consider the issue of active pump control either in this paper, which defines a significant research topic on its own [29], and spare it as a topic for future research, although pump flow-supplying capacity limitation is incorporated into our control design.

We first derive the hydraulic model of the MCV including realistic valve/cylinder models, multiple switching components connected to each valves, and two flow supply pumps with limited flow-providing capacities. These flow supply limits imply a fundamental limitation that the bucket could not be controlled as fast as we want. In order to circumvent this limitation, we design a novel velocity-field control law for the bucket position and orientation, which, by relying on a constrained optimization formulation, can adjust the velocity-field following speed of the bucket reflecting the physical constraints imposed by the MCV in such a way that it fully follows the desired velocity-field when the constraints are inactive and still preserves the desired bucket motion direction (or its automatic stopping) even when the constraints become active (e.g. flow supply limit) with the following-speed automatically slowing down. We further show that this constrained optimization can be real-time solved in a divide-and-conquer manner, with each step requiring to solve only two one-dimensional equations via only several Newton-Raphson iterations and also with the solution existence/optimality (or suboptimality) of the optimization problem always guaranteed. To validate our theoretical result, we also perform simulation study using the detailed hydraulic model implemented with Sim-Hydraulics.

The rest of this paper is organized as follows. We introduce the velocity-field control objective for the autonomous excavator with a brief system description, while elucidating challenges imposed by the MCV in Sec. 2. We then present the modeling of the MCV in Sec. 3. The main result of this paper, i.e., velocity-field control of excavator with MCV based on constrained-optimization, is presented in Sec. 4 with its solution procedure and properties elucidated there as well. Simulation results using a detailed excavator model with Simulink/Sim-Hydraulics is then presented in Sec. 5, followed by some concluding remarks in Sec. 6.

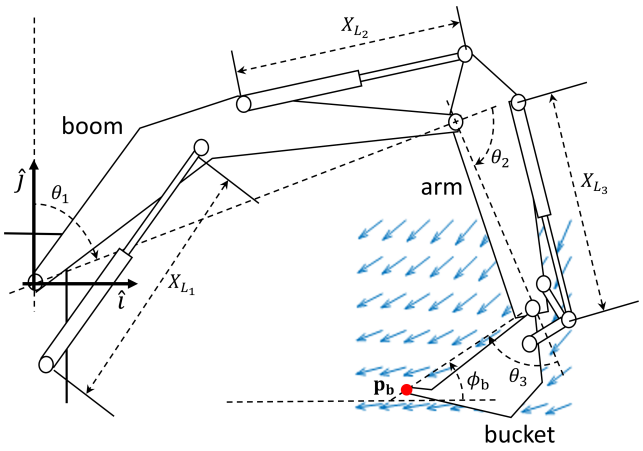

Fig. 2. Kinematics of the excavator with the angles θ_i and the cylinder strokes X_{L_i} of the bucket, arm and boom; and the velocity-field for the bucket position/orientation control.

2 Problem Formulation

The goal of this paper is to achieve the velocity-field control [23] of autonomous excavators as illustrated in Fig. 2, where the bucket position $\mathbf{p_b} \in$E(2) and its angle $\phi_b \in$S (expressed in an inertial frame) are desired to follow the *direction* of certain velocity-field (i.e. collection of velocity vectors defined at each bucket pose $(\mathbf{p_b}, \phi_b) \in$SE(2)), which is designed to encode some task objectives (e.g. level grading of Fig. 2). The issue of how to design this velocity-field is beyond the scope of this paper and we refer readers to, e.g., [14,23], where a velocity-field design scheme using variation of task-encoding potential functions and its real-time implementation are presented. Here, we focus only on the tasks in the sagittal plane (i.e. involving only bucket, arm and boom motion), as the swing motion is typically controlled by a separate swing hydraulic actuator and can be easily incorporated into the framework proposed here. The objective of this velocity-field control can then be written as

$$\mathbf{v_b} \to \lambda \cdot \mathbf{v_b^d}(\mathbf{p_b}, \phi_b) \tag{1}$$

where $\mathbf{v_b} := (\dot{\mathbf{p}}_\mathbf{b}; \dot{\phi}_b) \in$ se(2), $\mathbf{v_b^d}$: SE(2)$\to$se(2) is a map assigning the velocity-field vector $\mathbf{v_b^d} := (\dot{\mathbf{p}}_\mathbf{b}^\mathbf{d}; \dot{\phi}_b^d) \in$ se(2) at each pose of the bucket $(\mathbf{p_b}, \phi_b) \in$ SE(2), and $\lambda \in [0, 1]$ is the scaling factor to adjust the bucket speed whenever necessary (e.g. pump saturation) while still maintaining the direction of the desired velocity-field $\mathbf{v_b^d}$.

We choose this velocity-field control for autonomous excavators, since it allows for smooth task recovery in the presence of in-earth obstacles during the digging. For instance, when the bucket starts to pull obstacles (e.g. loosen rocks), it first slows down (i.e. λ decreasing), yet, still maintains the desired task direction (see Sec. 5.2 for more details); and, even when those objects completely stop the bucket (i.e. $\lambda = 0$: e.g., rocks stuck in holes) for a while and suddenly detach from the ground, the bucket can still maintain the desired task direction [1] (i.e. velocity-field direction) with its speed also gradually increasing. This smooth task recovery capability, we believe, would be very useful not only to achieve performance excavation but also to improve operation safety, which is becoming even more crucial for autonomous excavators, where, with no experienced operators on-board, it would be difficult to immediately and effectively suppress unsafe/dangerous situations autonomously. Note that this smooth task recovery is in general not possible with the standard trajectory tracking control (with time parameter t) or path following control (with progression parameter s), particularly when the desired trajectory/path is not a straight-line, since the accumulated tracking error (or following error, unless progression of s is reactively modulated [22, 36]) can induce excessively large control action possibly along a wrong direction when the objects are suddenly moved. Note that, the case of non-vanishing obstacles can be in general addressed only with human-user intervention, given the current state-of-the-art of autonomous systems.

Remark 1 Our framework proposed in this manuscript differs from the standard path following control, e.g., in the following two reasons: 1) our velocity field control encodes the direction of the velocity at each pose to converge to the integral curve, which only adjusts one variable λ to slow down, yet, the standard path following control encodes the separate motions in the tangential and normal directions to the desired path [3] with no direction of the velocity encoded *a priori*, which requires adjusting two variables, the tangential and normal speeds, to slow down, thus, further requires complicated coordination between them; and 2) the standard path following control, particularly those in robotics, typically assume the velocity bound (i.e. $\lambda_{\max}$) given [22,36], which, yet, for the autonomous excavator in this paper, can only be correctly identified by solving the complex MCV circuitry equations, that has never been done in other works and is done in this paper for the first time. In fact, the analysis of this complex MCV circuitry with multiple valves and without linearization is the main contribution of this paper.

For the autonomous excavator of Fig. 2, its Jacobian relation can be written by:

$$\mathbf{v_b} = J(\mathbf{X_L})\mathbf{V_L} \tag{2}$$

where $\mathbf{X_L} = (X_{L_1}; X_{L_2}; X_{L_3}) \in \Re^3$ and $\mathbf{V_L} = \dot{\mathbf{X}}_\mathbf{L} = (V_{L_1}; V_{L_2}; V_{L_3}) \in \Re^3$ are the strokes and the velocities of the boom, arm and bucket cylinders. Here, we focus only the excavation operations without triggering

[1] Recall that the integral curves of the two vector-fields, $\mathbf{v_b^d}(\mathbf{p_b}, \phi_b)$ and $\lambda \cdot \mathbf{v_b^d}(\mathbf{p_b}, \phi_b)$, are the same whenever $\lambda > 0$.

the singularity (i.e., $\theta_2 = 0, \pi$) of the Jacobian matrix $J(\mathbf{X_L}) \in \Re^{3\times3}$, which is rather easy to attain since: 1) the excavator is only of 3-DOF with no redundancy; and 2) the operation design and its velocity-field generation can be done before the operation, not in a reactive manner. Then, the velocity-field (1) can be mapped for the cylinder velocities, s.t.,

$$\mathbf{V_L} \to \lambda \cdot \mathbf{V_L^d} := \lambda \cdot J^{-1}(\mathbf{X_L})\mathbf{v_b^d}(\mathbf{p_b}(\mathbf{X_L}), \phi_b(\mathbf{X_L})) \quad (3)$$

which implies that, to attain the velocity-field control objective (1), we need to control the in-flow rate of the each cylinder $Q_{\text{in},i}$, $i = 1, 2, 3$, according to the desired velocity-field $\lambda\mathbf{V_L^d}$ defined at each configuration $\mathbf{X_L}$. For this, similar to other works (e.g. [1, 7, 8, 11, 17, 20, 21, 25, 28, 33]), we consider the spool position x_i, $i = 1, 2, 3$, of the directional valve of each cylinder as the control actuation, assuming that its dynamics is much faster than the excavator dynamics with a good-enough low-level spool position controller already embedded. Adequacy of this fast spool dynamics assumption and the robustness of our framework against that are verified by the detailed simulations in Sec. 5. We also assume that the cylinder stroke sensing is available (e.g. electromagnetic sensor [13], optical encoder [12], inertial measurement unit [34]) so that we can measure $\mathbf{X_L}$ and determine the desired cylinder velocities $\mathbf{V_L^d}(\mathbf{X_L})$; along with the availability of the cylinder cap/rod-side chambers pressure sensing $P_{A,i}, P_{B,i}$, $i = 1, 2, 3$. For redundant excavators, we may also utilize many well-established techniques of robot kinematic control [31] to address such challenging issues as singularity, optimal motion allocation, joint limits, etc. This, however, is not the main concern of this paper (on the analysis of, and control design with, MCV) and we instead refer readers to [31] and references therein.

Differently from the majority of related results, where individual actuation of each cylinder is assumed (e.g. [1,4,6,7,16,17,20,24,25,27,32,33]), even with the stroke and pressure sensing, it is difficult to design the control x_i to produce the desired in-flow rate $Q_{\text{in},i}$ here due to the deployment of the MCV typical for industrial excavators [8, 11, 21, 28] as depicted in Fig. 3, since: 1) *Pump 2* is connected to the boom and bucket cylinders at the same time, inducing hydraulic coupling between them, although *Pump 1* is to the arm cylinder only; 2) the main four-way directional valve for each cylinder (i.e. *Bkt, Bm1, Am1*) embeds a flow regenerative check valve inside them (see Sec. 3.2 for more details), which cracks to prevent pump cavitation, yet, in a purely mechanical manner, thus, inducing hydraulic circuitry switching of the MCV, that can be neither set nor predicted *a prior*; 3) the two pumps are limited-capacity flow-providing swash plate pumps with their flow outputs $Q_{\text{p},j}$ depending on the resultant pressure $P_{\text{p},j}$ of the MCV circuit due to the internal leakage flow, thus, should be solved together with all the other components of the MCV while taking into account of their flow saturation as well. Here,

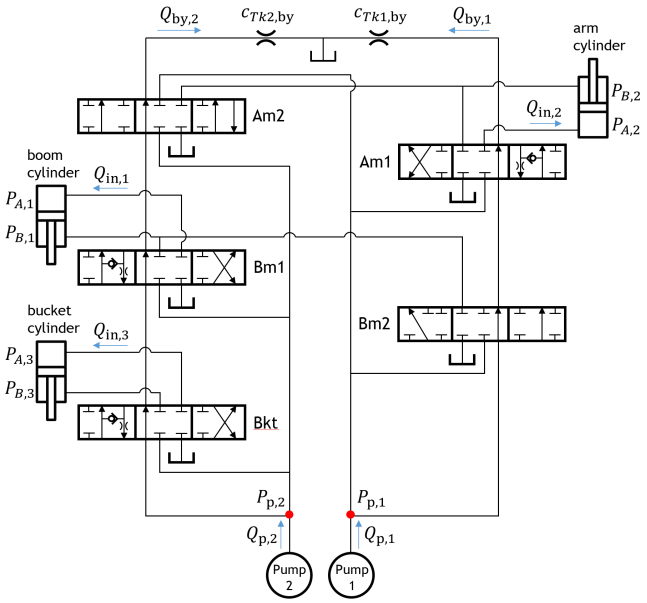

Fig. 3. Circuitry diagram of main control valve (MCV) of an industrial excavator with three cylinders and two pumps, with each cylinder controlled by asymmetric/nonlinear directional valve with regenerative valve inside to prevent pump cavitation, bypass conduit to save the pumping power, main pressure relief valve to prevent over pressurization (deactivated), and flow make-up valves (Am2, Bm2: deactivated).

we assume that the following valves are not activated: 1) the pressure relief valves, since they are activated only when some of the pumps get close to over-pressurization, which is rather a rare case; and 2) flow make-up valves (*Am2, Bm2*), since they are also activated only in rather rare situations requiring very large amount of flow for only-boom or only-arm motions [11]. We do not include priority valves either here, which are typically adopted for manual excavators to provide users with some feeling of operation.

The complexity imposed by the MCV as stated above then necessitates the holistic modeling and control design approach to attain the control objective (1) by incorporating all the components of the MCV system and their possible switching and saturations. This task, although seemingly daunting, by opportunistically utilizing relevant relations and constraints, can be reduced to rather simple divide-and-conquer iteration algorithm with each step requiring only solving two scalar equations and checking eight scalar inequalities. For this, we first start the modeling of the whole hydraulic circuit of the MCV system in Sec. 3.

3 Modeling of Main Control Valve

For the hydraulic modeling of the MCV in Fig. 3, we make the following standard assumption (e.g. [11, 26, 30]) that the fluid compressibility effect is negligible and the fluid dynamics is much faster than the excavator

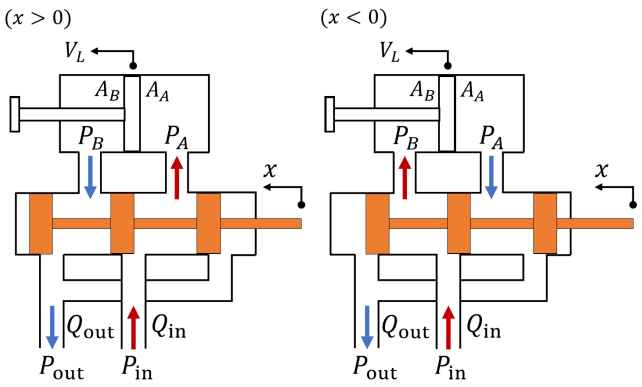

Fig. 4. Hydraulic cylinder controlled by a four-way directional valve with its spool position x.

mechanical dynamics. This assumption then allows us to use the flow volume conservation law, neglecting the compliance effect (e.g. fluid oscillation [4]), as well as the steady-state equation of the fluid dynamics (e.g. orifice equation) regardless of the cylinder motion.

3.1 Four-Way Directional Valve

Each cylinder of the MCV in Fig. 3 is actuated by its own four-way directional valve as shown in Fig. 4, where, with the positive spool position $x > 0$, the pump supply pressure P_{in} is connected into the cap-side A of the cylinder, with the in-flow rate to the cap-side and the out-flow rate from the rod-side B respectively denoted by Q_{in} and Q_{out}. This typically results in the cylinder extension $V_L > 0$ with $Q_{\text{in}} > 0$, although not always, particularly when the external loading on the cylinder is greater than the pump supply pressure (i.e. backflow). The out-flow rate Q_{out} is connected to P_{out}, which becomes the tank pressure (i.e. ambient pressure) when the regenerative circuit is not activated or that of the regenerative orifice before the tank when activated. For more details on this, see Sec. 3.2. The opposite, yet, similar, behavior happens when $x < 0$ as shown in Fig. 4.

Typical four-way directional valves used in industrial excavators, being optimized for performance, are nonlinear and asymmetric, with their effective opening area often obtained as shown in Fig. 5, where $A_{\text{v,in}}(x) \geq 0$ and $A_{\text{v,out}}(x) \geq 0$ are the effective valve opening area of the in-flow and out-flow routing depending on the spool position x (e.g. $A_{\text{v,in}}(x)$ from P_{p} to P_A and $A_{\text{v,out}}(x)$ from P_B to P_{out} when $x > 0$ and vice versa). As shown in Fig. 5, this real directional valve exhibits asymmetric deadband in its opening area, $x \in [-\delta_{\text{neg}}, \delta_{\text{pos}}]$, which yet is neglected in this paper, since this deadband is rather small, and, also, with the spool dynamics much faster than the excavator mechanical dynamics, passing this (small) deadband during short time interval does not significantly affect the excavator motion.

Let us consider the case of the positive spool position

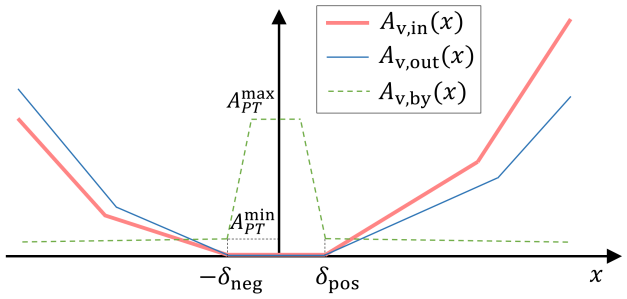

Fig. 5. Effective opening area of a typical asymmetric/nonlinear four-way directional valve and its internal bypass path as a function of the spool position x [11].

first (i.e. $x > 0$). The in-flow and out-flow rates can then be modeled by steady-state orifice equations s.t.

$$Q_{\text{in}} = \sqrt{\tfrac{2}{\rho}} C_d A_{\text{v,in}}(x) \sqrt{|P_{\text{in}} - P_A|} \text{sgn}\,(P_{\text{in}} - P_A) \tag{4}$$

$$Q_{\text{out}} = \sqrt{\tfrac{2}{\rho}} C_d A_{\text{v,out}}(x) \sqrt{|P_B - P_{\text{out}}|} \text{sgn}\,(P_B - P_{\text{out}}) \tag{5}$$

where ρ is the fluid density and C_d the discharge constant. Here, P_{in} is not constant, since the pump is flow-providing; and so is P_{out} with the activation of the regenerative valve. For more details for this, refer to Sec. 3.4 for the pump and Sec. 3.2 for the regenerative valve. Applying the flow volume rate conservation, we then have

$$\frac{Q_{\text{in}}}{A_A} = \frac{Q_{\text{out}}}{A_B} = V_L \tag{6}$$

where A_A and A_B are the cap/rod-side chamber piston areas with $A_A \neq A_B$ (i.e. asymmetric cylinder), and $V_L \in \Re$ is the cylinder piston velocity. Now, recall that for symmetric cylinders and linear/symmetric directional valve, we have the following flow-pressure equation [26]:

$$Q_{\text{L}} = c_L \cdot wx \cdot \sqrt{|P_{\text{s}} - P_L \text{sgn}\,(x)|} \text{sgn}\,(P_{\text{s}} - P_L \text{sgn}\,(x))$$

where $Q_{\text{L}} = Q_{\text{in}} = Q_{\text{out}}$, wx is the effective opening area with $A_{\text{v,in}}(x) = A_{\text{v,out}}(x) = wx$, $P_{\text{s}} := P_{\text{in}} - P_{\text{out}}$ is the valve differential supply pressure and $P_L := P_A - P_B$ is the differential load pressure. Our goal here is to derive a similar form as above for the asymmetric cylinder with the asymmetric/nonlinear directional valve, a proper incorporation of which is crucial to be applicable in practice, yet, can often substantially complicate the control synthesis. In contrast, our velocity-field control design, as presented in Sec. 4, can readily incorporate these aspects due to its form of constrained optimization.

Note first from (4)-(6) that

$$\text{sgn}\,(P_{\text{in}} - P_A) = \text{sgn}\,(P_B - P_{\text{out}}) = \text{sgn}\,(V_L)$$

with such terms as $A_{\mathrm{v,in}}(x), A_{\mathrm{v,out}}(x), A_A, A_B, C_d$ all non-negative. Then, applying (6), we have

$$P_{\mathrm{in}} - P_A = \frac{\rho A_A^2 V_L |V_L|}{2C_d^2 A_{\mathrm{v,in}}^2(x)}, \quad P_B - P_{\mathrm{out}} = \frac{\rho A_B^2 V_L |V_L|}{2C_d^2 A_{\mathrm{v,out}}^2(x)}$$

Similar to P_{s}, P_L above, define the differential supply force and the differential piston load force s.t.

$$F_{\mathrm{s}} := A_A P_{\mathrm{in}} - A_B P_{\mathrm{out}}, \quad F_L := A_A P_A - A_B P_B \tag{7}$$

We can then obtain the following equality:

$$\begin{aligned} F_{\mathrm{s}} - F_L &= A_A(P_{\mathrm{in}} - P_A) + A_B(P_B - P_{\mathrm{out}}) \\ &= \frac{\rho}{2C_d^2}\left[\frac{A_A^3}{A_{\mathrm{v,in}}^2(x)} + \frac{A_B^3}{A_{\mathrm{v,out}}^2(x)}\right] V_L^2 \mathrm{sgn}\,(V_L) \end{aligned}$$

from which, by noticing all the terms except $F_{\mathrm{s}} - F_L$ and $\mathrm{sgn}\,(V_L)$ are non-negative, we can further attain:

$$V_L(x, F_{\mathrm{s}}, F_L) = c_L(x)\sqrt{|F_{\mathrm{s}} - F_L|}\mathrm{sgn}\,(F_{\mathrm{s}} - F_L) \tag{8}$$

where

$$c_L(x) := \sqrt{\frac{2}{\rho}} C_d \left[\frac{A_A^3}{A_{\mathrm{v,in}}^2(x)} + \frac{A_B^3}{A_{\mathrm{v,out}}^2(x)}\right]^{-\frac{1}{2}} > 0 \tag{9}$$

This equation (8) means that the cylinder velocity V_L is determined by the spool position x and the valve supply force F_{s}, given the external piston load force F_L. Note also from (8) that, with $x > 0$, we will have $V_L > 0$ if $F_{\mathrm{s}} - F_L > 0$ (i.e. supply force F_{s} is greater than the piston load force F_L); whereas $V_L < 0$ if $F_{\mathrm{s}} - F_L < 0$ (i.e. back-flow).

For negative spool position $x < 0$, we can similarly obtain:

$$V_L(x, F_{\mathrm{s}}, F_L) = c_L(x)\sqrt{|F_{\mathrm{s}} + F_L|}\mathrm{sgn}\,(F_{\mathrm{s}} + F_L) \tag{10}$$

where

$$c_L(x) := -\sqrt{\frac{2}{\rho}} C_d \left[\frac{A_B^3}{A_{\mathrm{v,in}}^2(x)} + \frac{A_A^3}{A_{\mathrm{v,out}}^2(x)}\right]^{-\frac{1}{2}} < 0 \tag{11}$$

with F_{s}, Q_{in}, Q_{out} also modified to reflect the reserved routing of $P_{\mathrm{in}}, P_{\mathrm{out}}$ to the directional valve. Note that, with the closed spool position (i.e. $x = 0$), the cylinder velocity should be zero (i.e. $V_L = 0$), consistent with the fact that $c_L(0) = 0$ (after the deadband avoided as assumed in the second paragraph of Sec. 3.1). We can also easily check that $c_L(x)$ is continuous at $x = 0$ and also strictly increasing if the deadband is collapsed.

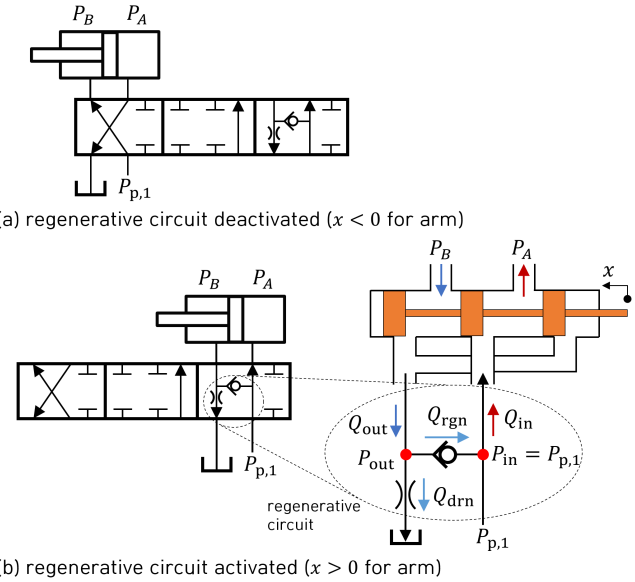

Fig. 6. Regenerative circuit (a) deactivated when $x < 0$ and (b) activated when $x > 0$ for arm four-way directional valve. Similarly, for boom/bucket four-way directional valves, deactivated when $x > 0$ and activated when $x < 0$.

Combining (8) and (10), we can then obtain the force-flow equation similar to the above pressure-flow equation s.t.,

$$\begin{aligned} &V_L(x, F_{\mathrm{s}}, F_L) \\ &= c_L(x)\sqrt{|F_{\mathrm{s}} - F_L \mathrm{sgn}\,(x)|}\mathrm{sgn}\,(F_{\mathrm{s}} - F_L \mathrm{sgn}\,(x)) \end{aligned} \tag{12}$$

where $c_L(x)$ is strictly increasing function w.r.t. x as stated above. This shows that, given F_{s} and F_L, we can control the cylinder motion V_L by adjusting the spool position x. The stroke of this spool, however, is limited in practice, i.e.,

$$|x| \le x_{\mathrm{m}} \tag{13}$$

for some $x_{\mathrm{m}} > 0$. Note here that the supply force F_{s} is not constant, since $(P_{\mathrm{in}}, P_{\mathrm{out}})$ are not constant either as stated after (5). Note also from Fig. 3 that $P_{\mathrm{in},2} = P_{\mathrm{p,1}}$ and $P_{\mathrm{in},1} = P_{\mathrm{in},3} = P_{\mathrm{p,2}}$ from the connection of the pumps via the MCV circuitry therein.

3.2 Regenerative Circuit

Main function of the regenerative circuit is to prevent excessive pump pressure drop and consequent pump cavitation by rerouting the tank flow to the pump side. This regenerative circuit is embedded in each four-way directional valve and activated when $x > 0$ (i.e. for extending) for the arm cylinder and when $x < 0$ (i.e. for retracting) for the boom and bucket cylinders. This is because such pump pressure drop can be particularly severe during, e.g., heavy material uploading operation, where the payload can further speed up the extending arm cylinder

and the retracting boom and bucket cylinders due to the kinematic structure of the excavator - see Fig. 2. This regenerative circuit can be conceptualized as in Fig. 6 for the arm cylinder: 1) when $x > 0$, the circuit is activated with the drain orifice and check valve engaged; 2) if the extension is further sped up by pulling load, P_A and $P_{\mathrm{p},1}$ drops, while P_{out} increases with the drain orifice; 3) when $P_{\mathrm{out}} > P_{\mathrm{p},1}$, the check valve opens and some tank flow is regenerated to the pump side, giving a rise to $P_{\mathrm{p},1}$. Similarly works it for the boom and bucket cylinders when $x < 0$.

This regenerative circuit, along with the MCV, significantly complicates the modeling and control of the autonomous excavator, since it further creates the hydraulic coupling, which is triggered purely mechanically, thus, cannot be set or predicted *a prior*. Even for full autonomous excavators with abundant electronic valves used, we believe this regenerative circuit would still be adopted due to its cost-effectiveness to prevent pump cavitation [30]. Now, we model this regenerative circuit in such a way that its behavior can be predicted given $(Q_{\mathrm{out}}, P_{\mathrm{in}})$, both which will also be predicted to attain the desired velocity-field control objective - see Sec. 4.

The flow volume conservation equation for the regenerative circuit in Fig. 6 is given by

$$Q_{\mathrm{out}} = Q_{\mathrm{rgn}} + Q_{\mathrm{drn}} \tag{14}$$

where

$$Q_{\mathrm{drn}} = c_d\sqrt{P_{\mathrm{out}}} \tag{15}$$

is the drain orifice flow rate with c_d being its flow coefficient; and

$$Q_{\mathrm{rgn}} = c_r\sqrt{P_{\mathrm{out}} - P_{\mathrm{in}}}\,\mathbf{1}(P_{\mathrm{out}} - P_{\mathrm{in}}) \tag{16}$$

is the regenerative flow rate through the check valve, which occurs only when $P_{\mathrm{out}} > P_{\mathrm{in}}$ with $\mathbf{1}(x) = 1$ if $x \geq 0$ and $\mathbf{1}(x) = 0$ otherwise; and c_r being its flow coefficient. Here, we assume $c_d < c_r$, since the drain orifice is typically more resistive than the regenerative check valve.

Combining (14)-(16), we then have:

$$Q_{\mathrm{out}} - c_d\sqrt{P_{\mathrm{out}}} = c_r\sqrt{P_{\mathrm{out}} - P_{\mathrm{in}}}\,\mathbf{1}(P_{\mathrm{out}} - P_{\mathrm{in}}) \tag{17}$$

where, given $(Q_{\mathrm{out}}, P_{\mathrm{in}})$, the LHS (left hand side) is strictly decreasing w.r.t. P_{out}, whereas the RHS (right hand side) increasing w.r.t. P_{out} from zero - see Fig. 7. From Fig. 7, we can then see that, given $(Q_{\mathrm{out}}, P_{\mathrm{in}})$,

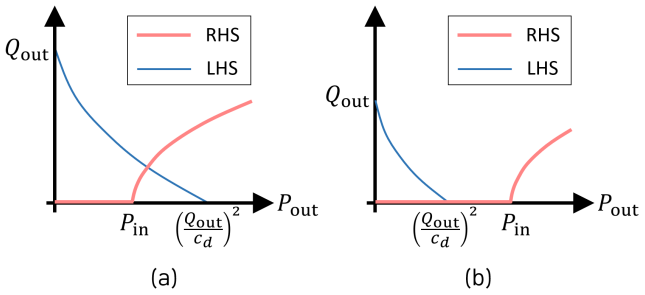

Fig. 7. Existence and uniqueness of the solution P_{out} of (17) given $(Q_{\mathrm{out}}, P_{\mathrm{in}})$: (a) when $P_{\mathrm{in}} < (Q_{\mathrm{out}}/c_d)^2$ (i.e. check valve open) and; (b) when $P_{\mathrm{in}} \geq (Q_{\mathrm{out}}/c_d)^2$ (i.e. check valve closed).

$\sqrt{P_{\mathrm{out}}}$ is uniquely determined by

$$\sqrt{P_{\mathrm{out}}} = \begin{cases} \frac{Q_{\mathrm{out}}}{c_d} & \text{if } P_{\mathrm{in}} \geq \frac{Q_{\mathrm{out}}^2}{c_d^2} \\ \frac{c_r\sqrt{Q_{\mathrm{out}}^2 + (c_r^2 - c_d^2)P_{\mathrm{in}}} - c_d Q_{\mathrm{out}}}{c_r^2 - c_d^2} & \text{otherwise} \end{cases}$$

$$=: f(Q_{\mathrm{out}}, P_{\mathrm{in}}) \tag{18}$$

where $c_r > c_d$. Here, note that finding this P_{out} surmounts to solve the regenerative circuit given $(Q_{\mathrm{out}}, P_{\mathrm{in}})$, since we can then fully characterize its behavior with the occurrence of check valve opening identified as well. Doing so only requires $(Q_{\mathrm{out}}, P_{\mathrm{in}})$, which are in turn to be estimated given the velocity-field control objective (1). This explicit solution of $P_{\mathrm{out}}(Q_{\mathrm{out}}, P_{\mathrm{in}})$ greatly simplifies our velocity-field control algorithm in Sec. 4 as compared to the approach of computing solutions for all possible opening and closing of all regenerative circuits and checking feasibility of each solution *a posterior*. This solution $P_{\mathrm{out}}(Q_{\mathrm{out}}, P_{\mathrm{in}})$ of the regenerative circuit has the following properties, which are to be used for Th. 3 later. For this, we also assume P_{in} as established in Prop. 2.

Proposition 1 *The function f defined in* (18) *possesses the following properties: 1) with $Q_{\mathrm{out}} \to 0$, $f(Q_{\mathrm{out}}, P_{\mathrm{in}}) \to 0$ and the regenerative check valve is closed; 2) $\frac{\partial f}{\partial Q_{\mathrm{out}}} \geq 0$; 3) $\frac{\partial f}{\partial P_{\mathrm{in}}} \geq 0$; and 4) $2f\frac{\partial f}{\partial P_{\mathrm{in}}} \leq 1$.*

PROOF. The first item is a direct consequence from (18), where $\sqrt{P_{\mathrm{out}}}$ converges to the first line of (18) (i.e. regenerative check valve is closed) if $Q_{\mathrm{out}} \to 0$ with $P_{\mathrm{in}} \geq 0$. The second item can be shown as follows. From (18), we have

$$\frac{\partial f}{\partial Q_{\mathrm{out}}} = \begin{cases} \frac{1}{c_d} & \text{if } P_{\mathrm{in}} \geq \frac{Q_{\mathrm{out}}^2}{c_d^2} \\ \frac{1}{c_r^2 - c_d^2}\left[\frac{c_r Q_{\mathrm{out}}}{\sqrt{Q_{\mathrm{out}}^2 + (c_r^2 - c_d^2)P_{\mathrm{in}}}} - c_d\right] & \text{otherwise} \end{cases}$$

which is decreasing w.r.t. P_{in} for $P_{\mathrm{in}} \leq (Q_{\mathrm{out}}/c_d)^2$,

implying that $\frac{\partial f}{\partial Q_{\rm out}} \geq \frac{\partial f}{\partial Q_{\rm out}}\Big|_{P_{\rm in}=(Q_{\rm out}/c_d)^2} = 0$ with $1/c_d > 0$. The third property follows from:

$$\frac{\partial f}{\partial P_{\rm in}} = \begin{cases} 0 & \text{if } P_{\rm in} \geq \frac{Q_{\rm out}^2}{c_d^2} \\ \frac{c_r}{2\sqrt{Q_{\rm out}^2+(c_r^2-c_d^2)P_{\rm in}}} & \text{otherwise} \end{cases} \geq 0$$

For the last property, we can obtain:

$$2f\frac{\partial f}{\partial P_{\rm in}} = \begin{cases} 0 & \text{if } P_{\rm in} \geq \frac{Q_{\rm out}^2}{c_d^2} \\ \frac{c_r}{c_r^2-c_d^2}\left[c_r - \frac{c_d Q_{\rm out}}{\sqrt{Q_{\rm out}^2+(c_r^2-c_d^2)P_{\rm in}}}\right] & \text{otherwise} \end{cases}$$

which is increasing w.r.t. $P_{\rm in}$ for $P_{\rm in} < \frac{Q_{\rm out}^2}{c_d^2}$, implying that $2f\frac{\partial f}{\partial P_{\rm in}} \leq 2f\frac{\partial f}{\partial P_{\rm in}}\Big|_{P_{\rm in}=(Q_{\rm out}/c_d)^2} = 1$.

3.3 Bypass Flow

As shown in Fig. 3, when the four-way directional valves are closed, the pump flow is then routed to the internal bypass path inside each of these directional valves, lowering the resultant pump pressure inside MCV, thereby, reducing the pumping work to save the energy. This internal bypass path in fact opens in a complementary manner with the directional valve opening as a function of the spool position x - see Fig. 5. Following Fig. 5, we can approximate this internal bypass path opening s.t.,

$$A_{\rm v,by}(x) = \begin{cases} A_{PT}^{\min} & \text{for } x \neq 0 \\ A_{PT}^{\max} & \text{for } x = 0 \end{cases} \tag{19}$$

with the spool deadband $x \in [-\delta_{\rm neg}, \delta_{\rm pos}]$ collapsed as stated in the second paragraph of Sec. 3.1. The flow coefficient of the orifice equation of this bypass path is then given by

$$c_{\rm v,by}(x) = \sqrt{\tfrac{2}{\rho}} C_d A_{\rm v,by}(x) =: \begin{cases} c_{\rm v,by}^{\min} & \text{for } x \neq 0 \\ c_{\rm v,by}^{\max} & \text{for } x = 0 \end{cases} \tag{20}$$

Now, consider the bypass flow from *Pump 1* through *Bm2*, *Am 1* and *Tk 1* orifice in Fig. 3. Its flow rate is then given by

$$Q_{\rm by,1} = c_{\rm by,1}(x_2)\sqrt{P_{\rm p,1}} \tag{21}$$

where x_2 is the arm spool position, and $c_{\rm by,1}$ is the composite flow coefficient defined by

$$\frac{1}{c_{\rm by,1}^2} := \frac{1}{c_{Am1,\rm by}^2(x_2)} + \frac{1}{c_{Bm2,\rm by}^2} + \frac{1}{c_{Tk1,\rm by}^2}$$

with $c_{Am1,\rm by}$, $c_{Bm2,\rm by}$, and $c_{Tk1,\rm by}$ being the flow coefficient of each component. Similarly, the flow rate of the bypass flow from *Pump 2* is given by

$$Q_{\rm by,2} = c_{\rm by,2}(x_1, x_3)\sqrt{P_{\rm p,2}} \tag{22}$$

where x_1, x_3 are the boom and bucket spool positions, and $c_{\rm by,2}$ is the composite flow coefficient defined by

$$\frac{1}{c_{\rm by,2}^2} := \frac{1}{c_{Bm1,\rm by}^2(x_1)} + \frac{1}{c_{Bkt,\rm by}^2(x_3)} + \frac{1}{c_{Am2,\rm by}^2} + \frac{1}{c_{Tk2,\rm by}^2}$$

where $c_{Bm1,\rm by}$, $c_{Bkt,\rm by}$, $c_{Am2,\rm by}$, and $c_{Tk2,\rm by}$ are the flow coefficients of each component. From (20), we have the following switching behavior: 1) $c_{\rm by,1}(x_2) = c_{\rm by,1}^{\min} > 0$ if $x_2 \neq 0$ and $c_{\rm by,1}(x_2) = c_{\rm by,1}^{\max} > c_{\rm by,1}^{\min}$ if $x_2 = 0$; and 2) $c_{\rm by,2}(x_1, x_3) = c_{\rm by,2}^{\min} > 0$ if $x_1 \neq 0$ and $x_3 \neq 0$, $c_{\rm by,2}(x_1, x_3) = c_{\rm by,2}^{{\rm mid},ij} > c_{\rm by,2}^{\min} > 0$ if $x_i \neq 0$ and $x_j = 0$, $(i,j) = \{(1,3),(3,1)\}$, and $c_{\rm by,2}(x_1, x_3) = c_{\rm by,2}^{\max} > c_{\rm by,2}^{{\rm mid},ij}$ if $x_1 = x_3 = 0$. This switching at $x_i = 0$ $(i = 1,2,3)$ will be incorporated in Sec. 4.2 for the feasibility analysis of the velocity-field control algorithm of Sec. 4.1.

3.4 Pump Flow Constraints

Applying the flow volume conservation, we can then attain the following two constraint equations for the MCV circuit in Fig. 3:

$$Q_{\rm p,1} = (Q_{\rm in,2} - Q_{\rm rgn,2}\mathbf{1}(x_2)) + Q_{\rm by,1} \tag{23}$$

$$Q_{\rm p,2} = \sum_{i=1,3} [Q_{{\rm in},i} - Q_{{\rm rgn},i}\mathbf{1}(-x_i)] + Q_{\rm by,2} \tag{24}$$

where $Q_{{\rm p},j}$ is the flow supply rate of the j-th pump $(j = 1,2)$, $Q_{{\rm in},i}$ is the in-flow rate to the i-th cylinder; and $Q_{{\rm rgn},i}$ is the regenerated flow through the i-th check valve, with $i = 1,2,3$ respectively associated with the boom, arm, and bucket actuators. Recall that the pressure relief valve and the make-up valves *Bm2* and *Am2* in Fig. 3 are assumed inactive (see Sec. 2), resulting in these two constituent relations (23)-(24) for the MCV system in Fig. 3.

In this paper, we assume each pump be a swash plate pump as typically deployed in industrial excavators, whose supply volume flow $Q_{{\rm p},j}$ can then be modelled as [2, 15]:

$$Q_{{\rm p},j} = v_{{\rm p},j} \cdot \omega_{{\rm p},j} \cdot \tan\alpha_{{\rm p},j} - q_{{\rm p},j}(P_{{\rm p},j}, \omega_{{\rm p},j}, \alpha_{{\rm p},j}) \tag{25}$$

where $v_{{\rm p},j}$ is the constant displacement volume of the pump, $\omega_{{\rm p},j}$ is the shaft rotation speed, $\alpha_{{\rm p},j}$ is the swash plate angle, $q_{{\rm p},j}$ is the internal leakage volume flow in the pump (via clearance), and $P_{{\rm p},j}$ is the pressure at

the supply port of the pump. The pump flow (25) then satisfies

$$\left.\frac{\partial Q_{\mathrm{p},j}}{\partial P_{\mathrm{p},j}}\right|_{(\alpha_{\mathrm{p},j},\omega_{\mathrm{p},j})=\text{constant}} = -\frac{\partial q_{\mathrm{p},j}}{\partial P_{\mathrm{p},j}} \leq 0 \tag{26}$$

since the internal leakage flow of the pump increases (or decreases, resp.) with the pressure at the pump $P_{\mathrm{p},j}$ increasing (or decreasing, resp.) [15]. We also assume that the pump is a constant-flow pump with $(\alpha_{\mathrm{p},j}, \omega_{\mathrm{p},j})$ constant or the pump dynamics (i.e., $(\alpha_{\mathrm{p},j}, \omega_{\mathrm{p},j})$) is slower enough than that of the MCV circuitry, so that (26) can be assumed for the control computation purpose in Sec. 4. Full inclusion of more sophisticated (or aggressive) active pump control, which itself defines a significant research topic [29], is beyond the scope of this paper and spared as a future research topic. In typical industrial excavators, $\alpha_{\mathrm{p},j}$ and $\omega_{\mathrm{p},j}$ are measured/monitored with swash plate actuating piston stroke sensors and pump crankshaft speed sensors. This measurement of $(\alpha_{\mathrm{p},j}, \omega_{\mathrm{p},j})$, along with the data-fitted leakage function $q_{\mathrm{p},j}$, is to be used in Sec. 4 to compute the required $P_{\mathrm{p},j}$ to generate the desired velocity-field control action (i.e., (39) with (27)-(28)).

With only the condition (26) assumed for the pump, we can then show that, given $(\mathrm{sgn}\,(x_i), Q_{\mathrm{in},i})$, the MCV constraint (23)-(24) can be solved with its solution being also unique as long as the velocity-field control objective (3) is permissible by the capacity of the supply pumps. See the next Prop. 2, which also presents some properties to be used for Th. 3 in Sec. 4.2. For this, note first that we can obtain from (14)-(15) and (18) that

$$Q_{\mathrm{rgn},i} = Q_{\mathrm{out},i} - c_{d,i}\sqrt{P_{\mathrm{out},i}} = Q_{\mathrm{out},i} - c_{d,i} f_i(Q_{\mathrm{out},i}, P_{\mathrm{p},j})$$

where f_i is defined in (18) for the i-th cylinder, $c_{d,i}$ is the flow coeffieicnt of the drain orifice, and $(i,j) = \{(2,1),(1,2),(3,2)\}$. Using $Q_{\mathrm{out},2} = \gamma_2 Q_{\mathrm{in},2}$ from (6) with $\gamma_i := A_{B_i}/A_{A_i}$, we can then rewrite (23) s.t.,

$$\begin{aligned} &Q_{\mathrm{in},2} + \left(-\gamma_2 Q_{\mathrm{in},2} + c_{d,2} f_2(\gamma_2 Q_{\mathrm{in},2}, P_{\mathrm{p},1})\right)\mathbf{1}(x_2) \\ &= Q_{\mathrm{p},1}(P_{\mathrm{p},1}) - c_{\mathrm{by},1}(x_2)\sqrt{P_{\mathrm{p},1}} \end{aligned} \tag{27}$$

and also similarly (24) s.t.,

$$\begin{aligned} &\sum_{i=1,3}\left[Q_{\mathrm{in},i} + \left(-\gamma_i^{-1} Q_{\mathrm{in},i} + c_{d,i} f_i(\gamma_i^{-1} Q_{\mathrm{in},i}, P_{\mathrm{p},2})\right)\mathbf{1}(-x_i)\right] \\ &= Q_{\mathrm{p},2}(P_{\mathrm{p},2}) - c_{\mathrm{by},2}(x_1, x_3)\sqrt{P_{\mathrm{p},2}} \end{aligned} \tag{28}$$

where $Q_{\mathrm{p},j}(P_{\mathrm{p},j})$ is given by (25) satisfying (26) with the constant (or measurable) $(\alpha_{\mathrm{p},j}, \omega_{\mathrm{p},j})$ and the data-fitted function $q_{\mathrm{p},j}$. We also have γ_i^{-1} for (28) instead of γ_i for (27), since the boom and bucket regenerative circuits are activated with $x_i < 0$ (i.e. during retraction), for which $Q_{\mathrm{in},i}$ is connected to the rod-side chamber rather than the cap-side chamber for (27). These equations (27)-(28) then show that the solvability of the MCV constraint equations (23)-(24) is equivalent to finding $P_{\mathrm{p},j}$ given $(\mathrm{sgn}\,(x_i), Q_{\mathrm{in},i})$ as a function of $Q_{\mathrm{in},i}$ satisfying (27)-(28), as summarized in the next Prop. 2.

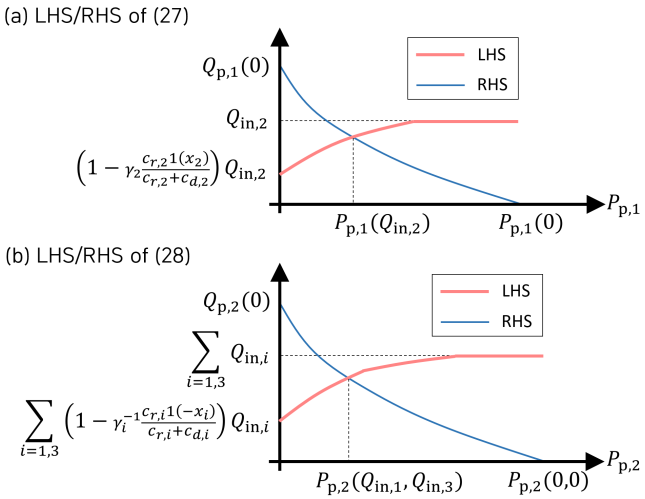

Fig. 8. Trajectories of the LHS and RHS and the solution existence condition of the MCV constituent equations: (a) for the arm circuit (27); and (b) for the boom/bucket circuit (28).

Proposition 2 *Suppose the supply flow of both Pump 1 and Pump 2 satisfies the property of* (26)*. Then, given* $(sgn\,(x_i), Q_{\mathrm{in},i})$ *and* $(V_{L_i}^d, P_{A,i}, P_{B,i})$*, the MCV constraint equations* (27)-(28) *assume unique solution* $P_{\mathrm{p},1}(Q_{\mathrm{in},2}) \geq 0$ *and* $P_{\mathrm{p},2}(Q_{\mathrm{in},1}, Q_{\mathrm{in},3}) \geq 0$ *if and only if*

$$\left(1-\gamma_2\frac{c_{r,2}\mathbf{1}(x_2)}{c_{r,2}+c_{d,2}}\right)Q_{\mathrm{in},2} \leq Q_{\mathrm{p},1}(0) \tag{29}$$

$$\sum_{i=1,3}\left(1-\gamma_i^{-1}\frac{c_{r,i}\mathbf{1}(-x_i)}{c_{r,i}+c_{d,i}}\right)Q_{\mathrm{in},i} \leq Q_{\mathrm{p},2}(0) \tag{30}$$

Further, these solutions $P_{\mathrm{p},1}(Q_{\mathrm{in},2})$ *and* $P_{\mathrm{p},2}(Q_{\mathrm{in},1}, Q_{\mathrm{in},3})$ *have the following properties: 1)* $\frac{\partial P_{\mathrm{p},1}(Q_{\mathrm{in},2})}{\partial Q_{\mathrm{in},2}} < 0$*; 2)* $\frac{\partial P_{\mathrm{p},2}(Q_{\mathrm{in},1},Q_{\mathrm{in},3})}{\partial Q_{\mathrm{in},i}} < 0$ *if* $x_i \geq 0$*, or if* $x_i < 0$ *and* $P_{\mathrm{p},2}(Q_{\mathrm{in},1}, Q_{\mathrm{in},3}) \geq \left(\frac{Q_{\mathrm{in},i}}{\gamma_i c_{d,i}}\right)^2$ *(*$i = 1, 3$*).*

PROOF. First, note that, given $\mathrm{sgn}\,(x_2)$ and $Q_{\mathrm{in},2}$, the LHS of (27) is non-decreasing w.r.t. $P_{\mathrm{p},1}$ with the minimum attained at $P_{\mathrm{p},1} = 0$, since $\frac{\partial f_2}{\partial P_{\mathrm{p},1}} \geq 0$ from Prop. 1. On the other hand, the RHS of (27) is non-increasing w.r.t. $P_{\mathrm{p},1}$ from (26) with its maximum attained at $P_{\mathrm{p},1} = 0$. See Fig. 8. This then implies that $P_{\mathrm{p},1}(Q_{\mathrm{in},2})$ is uniquely determined if and only if the LHS of (27) is less than the RHS of (27) at $P_{\mathrm{p},1} = 0$, which can be written by (29) using the definition of f_2 in (18). Similarly, we can obtain the condition (30) for (28).

Let us also differentiate (27) w.r.t. $Q_{\text{in},2}$. We can then have

$$\frac{\partial P_{\text{p},1}(Q_{\text{in},2})}{\partial Q_{\text{in},2}} = \frac{-1+\gamma_2\left(1-c_{d,2}\frac{\partial f_2}{\partial Q_{\text{out},2}}\right)\mathbf{1}(x_2)}{-\frac{\partial Q_{\text{p},1}}{\partial P_{\text{p},1}}+\frac{c_{\text{by},1}(x_2)}{2\sqrt{P_{\text{p},1}}}+c_{d,2}\frac{\partial f_2}{\partial P_{\text{p},1}}\mathbf{1}(x_2)} < 0$$

where the denominator is strictly positive, since $\partial Q_{\text{p},1}/\partial P_{\text{p},1} \leq 0$ (from (26)) and $\partial f_2/\partial P_{\text{p},1} \geq 0$ (from Prop. 1), and the nominator is strictly negative since $\gamma_2 < 1$ and $\partial f_2/\partial Q_{\text{out},2} \geq 0$ (from Prop. 1).

Similarly, differentiating (28) w.r.t. $Q_{\text{in},i}$, we have

$$\frac{\partial P_{\text{p},2}(Q_{\text{in},1},Q_{\text{in},3})}{\partial Q_{\text{in},i}} = \frac{-1+\frac{1}{\gamma_i}\left(1-c_{d,i}\frac{\partial f_i}{\partial Q_{\text{out},i}}\right)\mathbf{1}(-x_i)}{-\frac{\partial Q_{\text{p},2}}{\partial P_{\text{p},2}}+\frac{c_{\text{by},2}(x_1,x_3)}{2\sqrt{P_{\text{p},2}}}+\sum_{k=1,3}c_{d,k}\frac{\partial f_k}{\partial P_{\text{p},2}}\mathbf{1}(-x_k)} \quad (31)$$

where the denominator is strictly positive as above. This then implies that: 1) if $x_i > 0$, $\frac{\partial P_{\text{p},2}}{\partial Q_{\text{in},i}} < 0$; 2) if $x_i < 0$ and $P_{\text{p},2}(Q_{\text{in},1},Q_{\text{in},3}) > \left(\frac{Q_{\text{in},i}}{\gamma_i c_{d,i}}\right)^2 = \left(\frac{Q_{\text{out},i}}{c_{d,i}}\right)^2$, from the expression of $\frac{\partial f_i}{\partial Q_{\text{out},i}}$ in the proof of Prop. 1 with $P_{\text{in},i} = P_{\text{p},2}$, we have $\partial f_i/\partial Q_{\text{out},i} = 1/c_{d,i}$, resulting again to $\frac{\partial P_{\text{p},2}}{\partial Q_{\text{in},i}} < 0$. □

In Prop. 2, it is possible that $\frac{\partial P_{\text{p},2}}{\partial Q_{\text{in},i}} \geq 0$, if $x_i \leq 0$ yet $P_{\text{p},2}(Q_{\text{in},1},Q_{\text{in},3}) \leq \left(\frac{Q_{\text{in},i}}{\gamma_i c_{d,i}}\right)^2$, $i = 1,3$. For instance, if $P_{\text{p},2} = \left(\frac{Q_{\text{in},i}}{\gamma_i c_{d,i}}\right)^2$, we have $\frac{\partial f_i}{\partial Q_{\text{out},i}} = 0$ (from the expression in the proof of Prop. 1), thus, with $\frac{1}{\gamma_i} > 1$ and the denominator of (31) strictly positive, $\frac{\partial P_{\text{p},2}}{\partial Q_{\text{in},i}} > 0$.

This Prop. 2 means that, if $(V^d_{L_i}, P_{A,i}, P_{B,i})$ is given, the state of the whole MCV circuit of Fig. 3 can be parameterized solely by the in-flow rates $Q_{\text{in},i}$, $i = 1,2,3$, as long as they are permissible by the pump capacities in the sense of (29)-(30). Note that this inflow-parameterization of the MCV includes the switching of the regenerative circuits (Sec. 3.2), the pump supply pressures $P_{\text{p},j}$ (Prop. 2) and also the spool position x_i from (12) with $c_{L_i}(x_i)$ being strictly increasing as stated therein. An important ramification of this is that we can design the spool actuation x_i for the velocity-field control (3) solely as functions of $V^d_{L_i}$ under some assumptions and constraints. This greatly facilitates the velocity-field control design - see Sec. 4.1.

Note that the inequalities (29)-(30) constitute the constraints imposed on the possible cylinder speed $Q_{\text{in},i}$ by the limited flow capacity of the supply pumps (i.e. $Q_{\text{p},j}(0)$). This then means that the autonomous excavator may not be able to produce the desired bucket velocity $\mathbf{v_b^d}$ in (1), if it is too fast or under the load too large to be accommodated by the pump capacity. On the other hand, it is always possible simply to stop the excavator by closing all the spool valves (i.e. $x_i = 0$) with $\lambda = 0$ regardless of the desired velocity $\mathbf{v_b^d}$ or the external load. In the next Sec. 4, we present and analyze a novel velocity-field control law of the excavator, which aims to achieve the full velocity-field tracking of (3) with $\lambda = 1$ when doing so is permissible by (29)-(30), whereas, if not, slows down the bucket speed to be permissible by (29)-(30), yet, still maintains the desired direction of (3) with $\lambda < 1$, thereby, enhancing performance, robustness and safety of the autonomous excavator as explained in Sec. 2.

4 Velocity-Field Control Design

4.1 Constrained Optimization Formulation

As stated above, given $(\text{sgn}(x_i), V^d_{L_i}, P_{A,i}, P_{B,i})$, the two constituent equations (27)-(28) completely characterize the behavior of the MCV circuit of Fig. 3 as functions of $Q_{\text{in},i}$, as long as the the pump flow limit constraints (29)-(30) are granted. Due to those constraints, it may not be possible to follow $V^d_{L_i}$, yet, would still be possible to follow $\lambda V^d_{L_i}$ with $0 \leq \lambda < 1$ as stated in (3). Note also that this velocity-field control objective (3) can be written as

$$Q_{\text{in},i} \to \lambda \cdot Q^d_{\text{in},i}(\mathbf{X_L}) \quad (32)$$

where $Q^d_{\text{in},i}(\mathbf{X_L})$ is the cylinder in-flow rate corresponding to $V^d_{L_i}(\mathbf{X_L})$ in (3) as given by

$$Q^d_{\text{in},i} = A_{A_i} \cdot V^d_{L_i}\ \mathbf{1}(V^d_{L_i}) - A_{B_i} \cdot V^d_{L_i}\ \mathbf{1}(-V^d_{L_i}) \quad (33)$$

and, similarly, we also have

$$Q^d_{\text{out},i} = A_{B_i} \cdot V^d_{L_i}\ \mathbf{1}(V^d_{L_i}) - A_{A_i} \cdot V^d_{L_i}\ \mathbf{1}(-V^d_{L_i}) \quad (34)$$

The feasibility of this velocity-field control objective can then be checked by evaluating the constituent equations (27)-(28) with $Q_{\text{in},i} = \lambda Q^d_{\text{in},i}$ for $\lambda \in [0,1]$ given $(\text{sgn}(x_i), V^d_{L_i}, P_{A,i}, P_{B,i})$. The corresponding spool position input x_i can also be computed via (12) with V_{L_i} there given by $Q_{\text{in},i}$ and x_i determined from $c_{L_i}(x_i)$ there being strictly increasing, as long as the spool travel limit (13) is respected. This is the main idea of our velocity-field control algorithm as detailed below. For this, we also assume $(P_{A,i}, P_{B,i})$ be constant during the control algorithm computation, since the excavation dynamics is typically much slower than the hydraulic dynamics

and the spool position dynamics as stated in Sec. 2 and Sec. 3; and the algorithm computation itself is fairly fast (see the paragraph after (42)). To further remove the condition $\mathrm{sgn}(x_i)$, we also set

$$\mathrm{sgn}(x_i) \leftarrow \mathrm{sgn}\left(V_{L_i}^d\right) \tag{35}$$

which then will be compatible with $Q_{\mathrm{in},i} = \lambda Q_{\mathrm{in},i}^d$ only when the following "no back-flow condition" is met:

$$F_{\mathrm{s},i} - F_{L,i}\mathrm{sgn}(x_i) > 0 \tag{36}$$

i.e., the direction of the spool opening $\mathrm{sgn}(x_i)$ should be the same as the cylinder in-flow direction $\mathrm{sgn}(Q_{\mathrm{in},i}) = \mathrm{sgn}\left(\lambda \cdot Q_{\mathrm{in},i}^d\right) = \mathrm{sgn}\left(V_{L_i}^d\right)$. We now formulate the velocity-field control algorithm in a constrained optimization problem:

$$\begin{aligned}
&\underset{\lambda\in[0,1]}{\text{maximize}} \quad \lambda && (37)\\
&\text{subj. to} \quad \text{given } (V_{L_i}^d, P_{A,i}, P_{B,i}) \text{ and } F_{\mathrm{offset},i} > 0\\
&\qquad \mathrm{sgn}(x_i) \leftarrow \mathrm{sgn}\left(V_{L_i}^d\right)\\
&\qquad \text{compute } (Q_{\mathrm{in},i}^d, Q_{\mathrm{out},i}^d) \text{ from (33)-(34)}\\
&\qquad (Q_{\mathrm{in},i}, Q_{\mathrm{out},i}) \leftarrow \lambda(Q_{\mathrm{in},i}^d, Q_{\mathrm{out},i}^d) && (38)\\
&\qquad \text{check pump flow constraints (29)-(30)}\\
&\qquad \text{obtain } (P_{\mathrm{p},1}, P_{\mathrm{p},2}) \text{ from (27)-(28)} && (39)\\
&\qquad \text{compute } P_{\mathrm{out},i} \text{ from (18):} && (40)\\
&\qquad\quad \text{for } i = 1,3\text{: } P_{\mathrm{in},i} = P_{\mathrm{p},2}\\
&\qquad\qquad P_{\mathrm{out},i} = 0 \ \text{ if } \ V_{L_i}^d \geq 0\\
&\qquad\qquad P_{\mathrm{out},i} = f(Q_{\mathrm{out},i}, P_{\mathrm{in},i})^2 \ \text{ if } \ V_{L_i}^d < 0\\
&\qquad\quad \text{for } i = 2\text{: } P_{\mathrm{in},i} = P_{\mathrm{p},1}\\
&\qquad\qquad P_{\mathrm{out},i} = f(Q_{\mathrm{out},i}, P_{\mathrm{in},i})^2 \ \text{ if } \ V_{L_i}^d \geq 0\\
&\qquad\qquad P_{\mathrm{out},i} = 0 \ \text{ if } \ V_{L_i}^d < 0\\
&\qquad \text{compute } F_{\mathrm{s},i}, F_{L,i} \text{ from (7) with:} && (41)\\
&\qquad\quad F_{\mathrm{s},i} = A_{A_i}P_{\mathrm{in},i} - A_{B_i}P_{\mathrm{out},i} \ \text{ if } \ V_{L_i}^d \geq 0\\
&\qquad\quad F_{\mathrm{s},i} = A_{B_i}P_{\mathrm{in},i} - A_{A_i}P_{\mathrm{out},i} \ \text{ if } \ V_{L_i}^d < 0\\
&\qquad \text{check no back-flow condition:}\\
&\qquad\quad F_{\mathrm{s},i} - F_{L,i}\mathrm{sgn}(x_i) \geq F_{\mathrm{offset},i}\\
&\qquad \text{compute } x_i \text{ from (12)} && (42)\\
&\qquad \text{check spool travel limit (13)}
\end{aligned}$$

This constrained optimization (37) can be real-time solved in a divide-and-conquer manner, with each step requiring only to: 1) solve two scalar equations (27)-(28) via Newton-Raphson method, whose solution existence is always guaranteed (see Sec. 4.2) and which can also be solve fairly quickly (e.g. typically requires less than 10 iterations, running only 0.052ms with PC with 3.30GHz Chips and 16GB memory); and 2) check eight scalar inequalities, i.e., two pump flow limit constraints (29)-(30), three no back-flow conditions (36), and three spool travel limit constraints (13). Given a certain $\lambda \in [0,1)$, if feasible solution x_i can be found satisfying all of the constraints (29)-(30), (36), and (13), we then increase λ. On the other hand, given $\lambda \in (0,1]$, if any "check" conditions in the constrained optimization is not satisfied, we abort the optimization loop and decrease λ in a divide-and-conquer manner as stated in Sec. 4.3 and resume the solving process of the optimization with that decreased λ.

4.2 Solution Feasibility and Properties

Note that solving the constrained optimization (37) means to find the solution of the two MCV constituent equations (27)-(28) with λ sweeping in $[0,1]$, and check if it complies with the sign conditions $\mathrm{sgn}(x_i) = \mathrm{sgn}\left(V_{L_i}^d\right)$, the pump limit constraints (29)-(30), the no back-flow conditions (36), and the spool travel limits (13). An immediate question would then be if there always exists such a solution $\lambda \in [0,1]$ for this constrained optimization (i.e. feasibility) and how does this solution set look like (e.g. convexity). These feasibility and properties of the λ-solution of (37) are crucial to device a strategy to adjust λ for the maximization problem of (37) (e.g. divide-and-conquer algorithm of Sec. 4.3) as well as to decide which kind of optimization solvers to choose and how to use them for (37). The following Th. 3 shows that the constrained optimization (37) always assumes a convex solution set, which may be unique or can be characterized for some cases.

Theorem 3 *Consider the constrained optimization* (37) *of Sec. 4.1 with* $(V_{L_i}^d, P_{A,i}, P_{B,i}, F_{\mathrm{offset},i})$ *given. Suppose that each pump satisfies the following inequality: with* $sgn(x_i) = sgn\left(V_{L_i}^d\right)$,

$$\begin{aligned}
&[A_{A_i}\mathbf{1}(x_i) + A_{B_i}\mathbf{1}(-x_i)]P_{\mathrm{p},j}(0)\\
&\qquad > F_{L,i}sgn(x_i) + F_{\mathrm{offset},i}
\end{aligned} \tag{43}$$

where $(j,i) \in \{(1,2),(2,1),(2,3)\}$, *and* $P_{\mathrm{p},j}(0)$ *is the solution of* (27)-(28) *with* $Q_{\mathrm{in},i} = 0$ *and* $f_i = 0$ *(i.e. intersection of RHS with the x-axis of Fig. 8). Then, the followings hold:*

(1) there always exists $\lambda_{\min} \geq 0$ *s.t., any* $\lambda \in [0, \lambda_{\min}]$ *is feasible;*
(2) if $V_{L_1}^d \geq 0$ *and* $V_{L_3}^d \geq 0$*, no other feasible set exists other than* $\lambda \in [0, \lambda_{\min}]$*; and*
(3) if $V_{L_1}^d < 0$ *or* $V_{L_3}^d < 0$*, no other feasible set exists on* $[0, \lambda_r]$ *other than* $\lambda \in [0, \lambda_{\min}]$*, where* λ_r *is the minimum* $\lambda > 0$ *with which the regenerative check valve of the boom or the bucket is open.*

PROOF. We first show that $\lambda = 0$ with $x_i = 0$ is always a trivial solution. For this, note that, if $x_i = 0$, we have $(Q_{\mathrm{in},i}, Q_{\mathrm{out},i}) = \lambda(Q_{\mathrm{in},i}^d, Q_{\mathrm{out},i}^d) = 0$ with $\lambda = 0$. Then, the pump constraints (29)-(30) are trivially

satisfied with the unique solutions $(P_{\mathrm{p},1}, P_{\mathrm{p},2})$ for the MCV constituent equations (27)-(28). Further, the no back-flow condition (36) becomes irrelevant, since we do not need to enforce (36) with $x_i = 0$. This $x_i = 0$ also trivially satisfies the spool travel limit constraint (13).

Let us consider the case of $\lambda \to 0$. With this $\lambda \to 0$, the pump constraints (29)-(30) are again trivially granted, with the unique solution of $P_{\mathrm{p},1}(Q_{\mathrm{in},2}) \geq 0$ and $P_{\mathrm{p},2}(Q_{\mathrm{in},1}, Q_{\mathrm{in},3}) \geq 0$ also given for the MCV constituent equations (27)-(28). We can also see that this solution $P_{\mathrm{p},1}(Q_{\mathrm{in},2})$ and $P_{\mathrm{p},2}(Q_{\mathrm{in},1}, Q_{\mathrm{in},3})$ satisfies the no back-flow conditions (36), that is, e.g., for $x_i > 0$, with (43),

$$A_{A_i} P_{\mathrm{in},i} - A_{B_i} P_{\mathrm{out},i} > F_{L_i} \mathrm{sgn}\,(x_i) + F_{\mathrm{offset},i} \tag{44}$$

where, with $\lambda \to 0$, $P_{\mathrm{in},i} \to P_{\mathrm{p},j}(0)$ and $P_{\mathrm{out},i} \to 0$ (from the item 1 of Prop. 1 with $Q_{\mathrm{out},i} = \gamma_i Q_{\mathrm{in},i}$ or $Q_{\mathrm{out},i} = \gamma_i^{-1} Q_{\mathrm{in},i}$). The spool limit constraints (13) are also always satisfied with $\lambda \to 0$, since from (12), we have

$$|c_{L_i}(x_i)| \sqrt{F_{\mathrm{offset},i}} \leq |\lambda V_{L_i}^d| \to 0$$

as $\lambda \to 0$ with (44), where $F_{\mathrm{offset},i} > 0$ is a given number. The case of $x_i < 0$ can be proceeded in a similar manner.

Next, we show the convexity of the solution set including $\lambda = 0$. For this, let us see what will happen if we increase λ from zero. From the continuity of the pump flow constraints (29)-(30), note first that there will be $\lambda > 0$, which still satisfies (29) and (30) simultaneously. This λ may not comply with the other constraints yet. To check this, let us consider the no back-flow condition (44) for the arm cylinder with $x_2 > 0$ (i.e. regenerative circuit engaged). Then, if we increase λ, $P_{\mathrm{in},i}$ decreases whereas $P_{\mathrm{out},i}$ increases, since $\frac{\partial P_{\mathrm{in},i}}{\partial Q_{\mathrm{in},i}} < 0$ (from Prop. 2) and $\frac{\partial P_{\mathrm{out},i}}{\partial Q_{\mathrm{in},i}} \geq 0$ (from Prop. 1 with $Q_{\mathrm{in},i} = \gamma_i^{-1} Q_{\mathrm{out},i}$). On the other hand, for the force-flow equation (12), we have

$$\lambda V_{L_i}^d = c_{L_i}(x_i) \sqrt{|F_{\mathrm{s},i} - F_{L,i} \mathrm{sgn}\,(x_i)|} \mathrm{sgn}\,(F_{\mathrm{s},i} - F_{L,i}) \tag{45}$$

where, again, given $(V_{L_i}^d, P_{A,i}, P_{B,i})$, as λ increases, $F_{\mathrm{s},i}$ decreases as shown above (from (44)), requiring $|x_i|$ to increase. The same conclusion can also be similarly attained for the case of $x_2 < 0$, for which we have $P_{\mathrm{out},i} = 0$ with no regenerative circuit engaged. This then means that, if we only consider the arm cylinder, there exists $\lambda_{\mathrm{min},2} \in (0, 1]$ s.t., the solution set is given by a convex set $[0, \lambda_{\mathrm{min},2}]$.

The complete solution set of the constrained optimization (37), yet, relies not only on the arm cylinder circuit, but also the bucket and boom circuit as well (i.e. $i = 1, 3$ with $P_{\mathrm{in},i} = P_{\mathrm{p},2}$), whose solution set is now analyzed. Similar as before, denote a solution of (29) and (30) by $\lambda \in (0, 1]$, and consider the no back-flow condition (36) for the following two cases.

Case 1 ($V_{L_1}^d \geq 0$ and $V_{L_3}^d \geq 0$): For this case, we have $x_1 \geq 0$ and $x_3 \geq 0$. The no flow-back condition is then given by the same form as (44). Then, similar as before, with $\frac{\partial P_{\mathrm{in},i}}{\partial Q_{\mathrm{in},i}} < 0$ (from Prop. 2) and $\frac{\partial P_{\mathrm{out},i}}{\partial Q_{\mathrm{in},i}} \geq 0$ (from Prop. 1 with $Q_{\mathrm{in},i} = \gamma_i Q_{\mathrm{out},i}$), we have that, if we increase λ, $P_{\mathrm{in},i}$ decreases while $P_{\mathrm{out},i}$ increases. We also have the same force-flow equation (45) again here, thus, if λ increases, x_i should increase. This then implies that there exist $\lambda_{\mathrm{min},1}, \lambda_{\mathrm{min},3} \in (0, 1]$ s.t., the solution set is given by a convex set, that is intersection of $[0, \lambda_{\mathrm{min},1}]$ and $[0, \lambda_{\mathrm{min},3}]$. Combining the conclusion above for the arm cylinder, we can then say that, if $V_{L_1}^d \geq 0$ and $V_{L_3}^d \geq 0$, the solution set of the constrained optimization (37) is given by $[0, \lambda_{\min}]$ with $\lambda_{\min} := \min(\lambda_{\mathrm{min},1}, \lambda_{\mathrm{min},2}, \lambda_{\mathrm{min},3})$ and no other solution set exists (i.e. item 2 of Th. 3).

Case 2 ($V_{L_1}^d < 0$ or $V_{L_3}^d < 0$): For this case, we have $x_1 < 0$ or $x_3 < 0$, thus, from Prop. 2, we have $\frac{\partial P_{\mathrm{in},i}}{\partial Q_{\mathrm{in},i}} < 0$ only when $P_{\mathrm{in},i} \geq \left(\frac{Q_{\mathrm{in},i}}{\gamma_i c_{d,i}}\right)^2$, and the term becomes sign-indetermined otherwise. Here, recall from (18) that this condition $P_{\mathrm{in},i} \geq \left(\frac{Q_{\mathrm{in},i}}{\gamma_i c_{d,i}}\right)^2$ in fact implies the regenerative check valve be closed. On the other hand, recall also from the item 1 of Prop. 1 that, if $Q_{\mathrm{out},i} \to 0$ (i.e. $\lambda \to 0$), $P_{\mathrm{out},i} \to 0$ with the regenerative check valve closed. Let us increase λ from such small enough value so that the pump flow constraint (30) is met and also at the same time the regenerative check valve is closed with $P_{\mathrm{in},i} > \left(\frac{Q_{\mathrm{in},i}}{\gamma_i c_{d,i}}\right)^2$. If we increase this λ, we then again have $\frac{\partial P_{\mathrm{in},i}}{\partial Q_{\mathrm{in},i}} < 0$ (from Prop. 2) and $\frac{\partial P_{\mathrm{out},i}}{\partial Q_{\mathrm{in},i}} \geq 0$ (from Prop. 1 with $Q_{\mathrm{in},i} = \gamma_i^{-1} Q_{\mathrm{out},i}$), implying that $P_{\mathrm{in},i}$ will decrease whereas $P_{\mathrm{out},i}$ increase. This then means that, similar as above, if we increase λ, the margin for the no back-flow condition (similar to (36)) and the regenerative check valve closing condition (i.e. $P_{\mathrm{in},i} > \left(\frac{\lambda Q_{\mathrm{in},i}^d}{\gamma_i c_{d,i}}\right)^2$) will reduce and eventually be violated, whereas the required spool position from (45) increases as well. From this, we can then conclude that: 1) the solution set is still given by $[0, \lambda_{\min}]$ which is convex on the region upper-bounded by λ_r that violates $P_{\mathrm{in},i} > \left(\frac{\lambda Q_{\mathrm{in},i}^d}{\gamma_i c_{d,i}}\right)^2$ (i.e. regenerative check valve opens); and 2) we do not know whether another solution set exists in $\lambda \in (\lambda_r, 1]$ if $\lambda_r < 1$, since, if once $P_{\mathrm{in},i} < \left(\frac{\lambda Q_{\mathrm{in},i}^d}{\gamma_i c_{d,i}}\right)^2$, the sign of $\frac{\partial P_{\mathrm{in},i}}{\partial Q_{\mathrm{in},i}}$ is indetermined. The item 3 of Th. 3 then follows along with the item 1 as well by combining the item 2 and item 3. □

The pump control assumption (43) simply means that each pump is strong enough to enable the excavator to perform the desired task under various external loading conditions $(P_{A,i}, P_{B,i})$. Note that $P_{\mathrm{p},j}(0)$ in (43) can be chosen by solving

$$Q_{\mathrm{p},j}(P_{\mathrm{p},j}(0)) = v_{\mathrm{p},j}\alpha_{\mathrm{p},j}\omega_{\mathrm{p},j} - q_{\mathrm{p},j}(P_{\mathrm{p},j}(0)) = c_{\mathrm{by},j}^{\min}\sqrt{P_{\mathrm{p},j}(0)}$$

with $P_{\mathrm{p},j}(0)$ assumed to be large enough to grant (43). From the above Th. 3, we can also see that: 1) the constrained optimization (37) always has a small enough feasible solution $\lambda_{\min} \in (0, 1]$, implying that the excavator can follow any desired bucket velocity $\mathbf{v_b^d}(\mathbf{X_L}) \in \Re^3$ by sufficiently scaling down the following speed; and 2) there always exists a convex solution set including $\lambda = 0$, thus, we can always find a local optimum close to $\lambda = 0$. Using this feasibility and solution set convexity, in the next Sec. 4.3, we propose a divide-and-conquer type solver for the constrained optimization (37) and analyze its convergence behavior.

4.3 Solution Algorithm for the Optimization

Given $(V_{L_i}^d, P_{A,i}, P_{B,i}, F_{\mathrm{offset},i})$, we solve the optimization problem (37) with a given tollerance $\epsilon > 0$, by iteratively updating its optimization variable λ via a divide-and-conquer algorithm in Alg. 1, whose main idea is to find an optimal solution by increasing (or decreasing) λ when it is feasible (or infeasible, resp.) that is already introduced at the last paragraph of Sec. 4.1. The following Th. 4 shows that we can always find the optimal (or loaclly optimal) solution of the constrained optimization (37) via this Alg. 1, owing to the convex (or locally convex, resp.) shape of the feasible set (from the Th. 3).

Algorithm 1 Divide-and-conquer algorithm

```
1: procedure DIV-CON(V^d_{L_i}, P_{A,i}, P_{B,i}, F_{offset,i}, ε)
2:     λ ← 1 and Δλ ← 1
3:     if λ = 1 is feasible for (37) then
4:         return λ = 1
5:     else
6:         while Δλ > ε do
7:             Δλ ← 0.5Δλ
8:             if λ is infeasible for (37) then
9:                 λ ← λ − Δλ
10:            else
11:                λ ← λ + Δλ
12:        if λ is feasible for (37) then
13:            return λ
14:        else
15:            return λ ← λ − Δλ
```

Theorem 4 *Consider the constrained optimization* (37) *of Sec. 4.1 with* $(V_{L_i}^d, P_{A,i}, P_{B,i}, F_{\mathrm{offset},i})$ *given, and suppose the condition* (43) *of Thm. 3 is met. Suppose the optimization variable* λ *is iteratively updated via the divide-and-conquer algorithm described in Alg. 1 with given* $\epsilon > 0$*. Then, the followings hold:*

(1) the Alg. 1 always returns $\lambda \in [0, 1]$ *with no more than* $N = \lceil -\log_2 \epsilon \rceil$ *times of iterations;*
(2) if $V_{L_1}^d \geq 0$ *and* $V_{L_3}^d \geq 0$, $|\lambda - \lambda^*| \leq \epsilon$, *where* $\lambda^* \in [0, 1]$ *is the global maximum of the constrained optimization* (37)*; and*
(3) if $V_{L_1}^d < 0$ *or* $V_{L_3}^d < 0$, $|\lambda - \lambda_{\mathrm{sub}}^*| \leq \epsilon$, *where* $\lambda_{\mathrm{sub}}^* \in [0, 1]$ *is some local maximum of the constrained optimization* (37)*.*

PROOF. If $\lambda = 1$ is feasible, the Alg. 1 returns $\lambda = 1$ with no iteration (from the line 4 of Alg. 1) (i.e. item 1 of Th. 4), which is the maximum solution of (37) (i.e. item 2 and 3 of Th. 4).

Let us consider the case that $\lambda = 1$ is infeasible so that the Alg. 1 proceeds into the iteration loop (i.e. the line 6 to 11 in Alg. 1). Let us denote the optimization variable λ and its update step $\Delta\lambda$ after the n-th iteration by $\lambda(n)$ and $\Delta\lambda(n)$ $(n \in \mathbb{N})$. Here, we have $\Delta\lambda(1) = 0.5$ (from the line 2, 7 of Alg. 1) and $\lambda(1) = 0.5$ (from the line 2, 9 of Alg. 1). We then have

$$\Delta\lambda(n) = 0.5^n \tag{46}$$

from the line 7 of Alg. 1. This implies lower/upper bounds for $\lambda(n)$ $(n \geq 2)$ s.t.

$$\lambda(n) \geq \lambda(1) - \sum_{l=2}^{n} \Delta\lambda(l) = 0.5^n > 0 \tag{47}$$

$$\lambda(n) \leq \lambda(1) + \sum_{l=2}^{n} \Delta\lambda(l) = 1 - 0.5^n < 1 \tag{48}$$

We also have $\Delta\lambda(N) = 0.5^N \leq \epsilon$ and $\Delta\lambda(N-1) = 0.5^{N-1} > \epsilon$ (from (46) and N defined in item 1 of Alg. 1), meaning that the iteration ends right after N-th iteration (from the line 6 of Alg. 1). The Alg. 1 then returns $\lambda(N)$ or $\lambda(N) - \Delta\lambda(N) = \lambda(N) - 0.5^N$ (from the line 13 or 15 of Alg. 1 and (46)), both of which are lower/upper bounded s.t. $\lambda(N) \in (0, 1)$ or $\lambda(N) - 0.5^N \in [0, 1)$ from (47), (48) (i.e. item 1 of Th. 4).

Suppose we have the $\lambda(N)$ feasible so that the Alg. 1 returns $\lambda(N)$ (from the line 13 of Alg. 1). Let us denote the last infeasible value of the optimization variable by $\lambda(m_1)$ $(0 \leq m_1 < N)$, where $\lambda(0) := 1$. Since $\lambda(m_1)$ is infeasible whereas $\lambda(l)$, $l = m_1 + 1, \cdots, N-1$, are feasible, we have (from the line 9, 11 of Alg. 1 and (46))

$$\begin{aligned}\lambda(N) &= \lambda(m_1) - \Delta\lambda(m_1+1) + \sum_{l=m_1+2}^{N} \Delta\lambda(l) \\ &= \lambda(m_1) - 0.5^{m_1+1} + \sum_{l=m_1+2}^{N} 0.5^l\end{aligned}$$

We then have $\lambda(N) + 0.5^N = \lambda(m_1)$, which is infeasible for the constraints of (37). Since $\lambda(N)$ is feasible whereas $\lambda(N) + 0.5^N$ is infeasible, there exists some local maximum $\lambda^*_{\rm sub} \in [\lambda(N), \lambda(N) + 0.5^N)$. This implies that $|\lambda(N) - \lambda^*_{\rm sub}| \leq 0.5^N \leq \epsilon$ (from the N defined in item 1 of Alg. 1).

Now suppose we have the $\lambda(N)$ infeasible so that the Alg. 1 returns $\lambda(N) - \Delta\lambda(N) = \lambda(N) - 0.5^N$ (from the line 15 of Alg. 1 and (46)). If some values of the optimization variable in the past iterations (i.e. $\lambda(l), l = 1, \cdots, N-1$) are feasible, let us denote the last feasible value by $\lambda(m_2)$ ($1 \leq m_2 < N$). Since $\lambda(m_2)$ is feasible whereas $\lambda(l)$, $l = m_2 + 1, \cdots, N-1$, are infeasible, we have (from the line 9, 11 of Alg. 1)

$$\begin{aligned}\lambda(N) &= \lambda(m_2) + \Delta\lambda(m_2+1) - \sum_{l=m_2+2}^{N} \Delta\lambda(l) \\ &= \lambda(m_2) + 0.5^{m_2+1} - \sum_{l=m_2+2}^{N} 0.5^l\end{aligned}$$

We then have $\lambda(N) - 0.5^N = \lambda(m_2)$, which is feasible for the constraints of (37). Since $\lambda(N) - 0.5^N$ is feasible whereas $\lambda(N)$ is infeasible, there exists some local maximum $\lambda^*_{\rm sub} \in [\lambda(N) - 0.5^N, \lambda(N))$. This implies that $|\lambda(N) - 0.5^N - \lambda^*_{\rm sub}| \leq 0.5^N \leq \epsilon$ (from the N defined in item 1 of Alg. 1). On the other hand, it is also possible that all of the past iteration values of the optimization variable (i.e. $\lambda(l), l = 1, \cdots, N-1$) are infeasible. If this is the case, we have (from the line 9 of Alg. 1)

$$\lambda(N) = \lambda(1) - \sum_{l=2}^{N} \Delta\lambda(l) = 0.5 - \sum_{l=2}^{N} 0.5^l = 0.5^N$$

Here, recall that the Alg. 1 returns $\lambda(N) - 0.5^N = 0$, which is always feasible (from the item 1 of Th. 3). Since $\lambda(N) - 0.5^N$ is feasible whereas $\lambda(N)$ is infeasible, there exist some local maximum $\lambda^*_{\rm sub} \in [\lambda(N) - 0.5^N, \lambda(N))$, which then also implies $|\lambda(N) - 0.5^N - \lambda^*_{\rm sub}| \leq 0.5^N \leq \epsilon$.

Now, consider the optimality of the local maximum $\lambda^*_{\rm sub}$ for (37) for the following two cases.

Case 1 ($V^d_{L_1} \geq 0$ and $V^d_{L_3} \geq 0$): For this case, recall that the feasible set of the constrained optimization (37) is convex (from the item 2 of Thm. 3). This means that the local maximum is as same as the global maximum, i.e., $\lambda^*_{\rm sub} = \lambda^*$ (i.e. item 2 of Th. 4).

Case 2 ($V^d_{L_1} < 0$ or $V^d_{L_3} < 0$): For this case, recall that, the feasible set of the constrained optimization (37) is convex on $[0, \lambda_r]$ (from the item 3 of Th. 3). This means that, if $\lambda_r \geq 1$, the feasible set of (37) is also convex on $[0, 1]$, implying that the local maximum $\lambda^*_{\rm sub} \in [0, 1]$ is as same as the global maximum, i.e., $\lambda^*_{\rm sub} = \lambda^*$. On the other hand, if $\lambda_r < 1$, the feasible set of (37) is possibly not convex on $[0, 1]$, which does not guarantee $\lambda^*_{\rm sub} = \lambda^*$ (i.e item 3 of Th. 4). $\square$

From the above Th. 4, we can see that: when $V^d_{L_1} \geq 0$ and $V^d_{L_3} \geq 0$ (or $V^d_{L_1} < 0$ or $V^d_{L_3} < 0$), the optimal solution (or a local maxima, resp.) of (37) is achieved with a specified tollerance $\epsilon > 0$ within a finite number of iteration N that is logarithmically increasing w.r.t. ϵ^{-1}. Note that, when $V^d_{L_1} < 0$ or $V^d_{L_3} < 0$, the final output of the Alg. 1 could exhibit chattering behavior along the proceeding control time steps, due to a change of a shape of the feasible set from the variation of $(V^d_{L_i}, P_{A,i}, P_{B,i}, F_{{\rm offset},i})$ along time, thus, possible switchings of convergence point $\lambda^*_{\rm sub}$ among multiple local maxima. However, this possibility of chattering is quite fundamental problem for non-convex optimization-based control techniques, thus, not discussed in this paper.

Remark 2 The proposed Alg. 1 as well as Th. 3 and Th. 4 are applicable even when the main pressure relief valve is activated, which we assumed inactive throughout this paper for simplicity. For this, recall that, the main pressure relief valve leaks some of the pump supply flow to the tank when the pump pressure $P_{{\rm p},j}$ exceeds the cracking pressure $P_{\rm pr}$, thereby, saturating the pump pressure $P_{{\rm p},j}$ to be $P_{{\rm p},j} \leq P_{\rm pr}$. This means that the pump flow constraints (23)-(24) are valid only when $P_{{\rm p},j} < P_{\rm pr}$ (i.e. relief valve inactive), whereas, if $P_{{\rm p},j} = P_{\rm pr}$ (i.e. relief valve activated), the pump flow constraints (23)-(24) are replaced by the pressure constraints $P_{{\rm p},j} = P_{\rm pr}$. This phenomenon can be analysed by Fig. 8 only with RHS curves on $P_{{\rm p},j} > P_{\rm pr}$ region replaced by a virtical line $P_{{\rm p},j} = P_{\rm pr}$ ($j = 1, 2$) and so their x-intercepts $P_{{\rm p},1}(0)$ and $P_{{\rm p},2}(0, 0)$ each replaced by $P_{\rm pr}$. This clearly implies that our proposed control algorithm is still applicable only with $P_{{\rm p},j}$ replaced by $\min\{P_{{\rm p},j}, P_{\rm pr}\}$ at (39) and so is our solution feasibility condition (43) only with $P_{{\rm p},j}(0)$ replaced by $P_{\rm pr}$. The proofs of Th. 3 and Th. 4 are also still valid for this case, since the core structure of the equations remains the same with this relief valve as explained here.

Remark 3 The proposed Alg. 1 as well as Th. 3 and Th. 4 are applicable even when the system setups are modificated, e.g., a check valve is added between the pump 1 (i.e. $P_{{\rm p},1}$) and the flow-inport of the arm spool valve (i.e. $P_{{\rm in},2}$). The added check valve in this case can be easily incorporated into the effective opening area of the spool valve by using the composition rule for the flow coefficients as used in the Sec. 3.3:

$$\frac{\rho}{2C_d^2 A^2_{\rm v,in,eff}(x)} = \frac{1}{c^2_{check}} + \frac{\rho}{2C_d^2 A^2_{\rm v,in}(x)}$$

where c_{check} is the flow coefficient of the check valve, and $A_{\mathrm{v,in,eff}}(x)$ is the effective opening area of the spool valve. The proofs of Th. 3 and Th. 4 are also still valid for this case with only $A_{\mathrm{v,in}}(x)$ replaced by $A_{\mathrm{v,in,eff}}(x)$. The second example of modification is to add a spool valve to make a 4-DOF excavator (or other machine), where the spool valves $i = 1, 3$ are connected to the pump 2 and $i = 2, 4$ to the pump 1. If the direction of the regenerative valve of $i = 4$ is as same as that of $i = 2$, the pump flow constraints (23)-(24) becomes:

$$Q_{\mathrm{p},1} = \sum_{i=2,4} \left[Q_{\mathrm{in},i} - Q_{\mathrm{rgn},i} \mathbf{1}(x_i) \right] + Q_{\mathrm{by},1}$$

$$Q_{\mathrm{p},2} = \sum_{i=1,3} \left[Q_{\mathrm{in},i} - Q_{\mathrm{rgn},i} \mathbf{1}(-x_i) \right] + Q_{\mathrm{by},2}$$

The only difference in this case is the numbers of indices, which implies the proofs of Th. 3 and Th. 4 are still applicable, since the core structure of the equations remains the same with this addition of spool valve here. Another example is the system having more or less number of pumps, which is similar to the second example.

5 Simulation

Simulations are performed to validate the control algorithm using a detailed Simulink/Sim-Hydraulics model. All of the hydraulic elements (see Fig. 3) and their modeling in Sec. 3 are included in this simulation model while the pressure relief valve and the make-up valves are assumed deactivated. This simulation model also includes a number of detailed phenomena in real excavators that are not considered in the modeling in the Sec. 3: 1) the second order spool dynamics with a time constant of 20ms [24], 2) the spool valve opening deadband inserted at $[-0.2x_{\mathrm{m}}, 0.2x_{\mathrm{m}}]$, 3) the fluid volume compliance and the flow resistance in the cylinder chambers/hoses, and 4) the manipulator dynamics/kinematics with the parameters similar to those of a commercial 22T excavator (i.e. boom/arm/bucket linkage length/inertia, cylinder-piston friction including Coulomb and viscous effect [32]). The linkages inertia with the fluid volume compliance creates natural frequencies ranging from 8∼15Hz, though the linkages are rigid and so their connecting joints not compliant. Here, the swash plate pump model is adopted with its swash plate angle and rotation speed maintained constant (i.e. constant flow) while the leakage flow increases proportionally/quadratically w.r.t. supply pressure [15].

Since the knowledges on the system are inaccurate in practice, we assume the model parameters used in the control algorithm to be uncertain: 1) the orifice flow coefficients on the regenerative circuits $c_{r,i}, c_{d,i}$ and on the bypass circuits $c_{Tk1,\mathrm{by}}, c_{Tk2,\mathrm{by}}$ are identified with ±33% errors; and 2) the spool valve opening function $c_{L_i}(x_i)$ is data fitted with (12) by calibrations with ±10% errors and its bypass conduit orifice $c_{Am1,\mathrm{by}}(x_2), c_{Bm1,\mathrm{by}}(x_1), c_{Bkt,\mathrm{by}}(x_3), c_{Am2,\mathrm{by}}, c_{Bm2,\mathrm{by}}$ are also calibrated with ±10% errors; and 3) the pump leakage function $q_{\mathrm{p},j}(P_{\mathrm{p},j}, \omega_{\mathrm{p},j}, \alpha_{\mathrm{p},j})$ is also data fitted by calibrations with ±10% errors.

We also assume the measurements used in the control algorithm to be inaccurate. Typical industrial pressure transducer models, which have a nominal range of $250bar$ with 3% bias due to transducer nonlinearity, temperature variation, and wear, are attached to the chamber hoses for chamber pressure sensing [33]. Here, we assume the pressure measurements also contain 2% noise after low pass filtering. The cylinder strokes are directly measured by optical encoders attached inside each cylinder chambers with $0.1mm$ resolution and $2.0mm$ bias due to wear.

The control commands (i.e. spool positions, x_i, $i = 1, 2, 3$) update rate is set as 100Hz for the simulation, which is a typical order for other autonomous excavators as well [17]. Note that, in each control time step, the constrained optimization (37) is solved via its solver Alg. 1 so that the optimal solution λ and its corresponding desired control commands x_i, $i = 1, 2, 3$, are calculated. Here, the error tollerance of the optimization solver Alg. 1 is chosen as $\epsilon = 10^{-7}$ in order to achieve sufficient accuracy and smoothness of the resulting optimal solution λ and its corresponding control inputs x_i, $i = 1, 2, 3$, along time. The Alg. 1 also runs no more than 24 iterations with this $\epsilon = 10^{-7}$, which requires only 1.25ms with 3.30GHz chips and 16GB memory, as each iteration can be very efficiently solved by: 1) solving two scalar equations via Newton-Raphson method, and 2) checking eight closed-form inequalities as explained in Sec. 4.1.

Here, for an illustrative example, the excavator is commanded to execute a digging motion following a rounded-rectangular trajectory $\mathbf{p_b^d}$ (blue dotted line in Fig. 9) with changing bucket tip angle w.r.t. the ground depending on its position s.t. $\phi_{\mathrm{b}}^d(\mathbf{p_b^d})$, linearly interpolated between $\phi_{\mathrm{b}}^d = 45°$at $p_{\mathrm{b,x}}^d = 3.5m$ and $\phi_{\mathrm{b}}^d = 120°$at $p_{\mathrm{b,x}}^d = 6.5m$, where $p_{\mathrm{b,x}}^d$ denotes the x-position of $\mathbf{p_b^d}$. This realistic desired bucket trajectory $(\mathbf{p_b^d}, \phi_{\mathrm{b}}^d)$ is designed regarding the workspace of the commercial 22T excavator based on its manipulator kinematics and cylinder stroke limits. We also design a velocity field (gray vector field in Fig. 9) that converges to this example trajectory so that the control algorithm Alg. 1 in Sec. 4 is given the desired bucket velocity $\mathbf{v_b^d}(\mathbf{p_b}, \phi_b)$ at each bucket pose. Simulation results with a soil disturbance/obstacle are then presented in the remainder of this section.

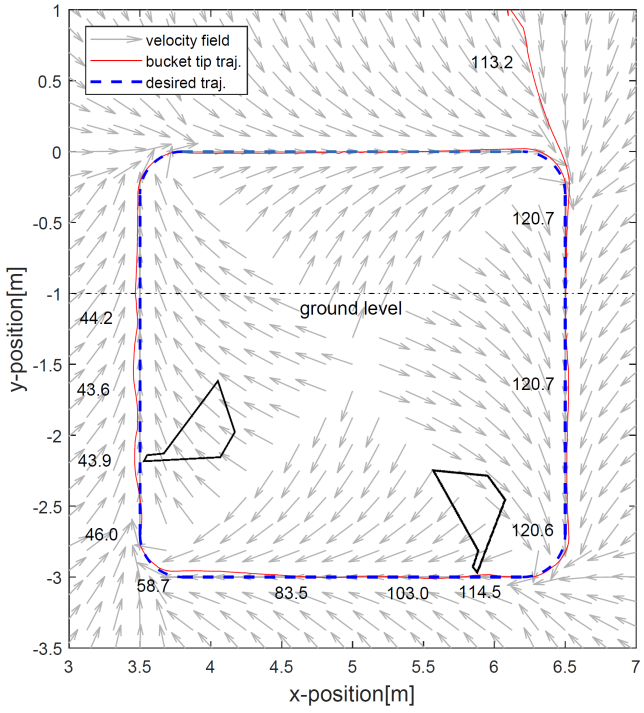

Fig. 9. The bucket tip position $\mathbf{p_b}$ trajectory (red line) and angle w.r.t. ground ϕ_b at every 5 seconds (numbers in degree along the red line) when bucket is moving in the soil disturbance. The coordinate system is as same as in Fig. 2.

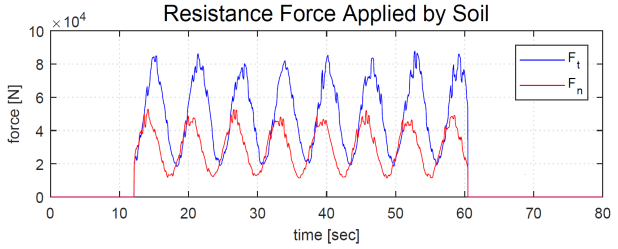

Fig. 10. Resistive force applied by soil to bucket tip.

5.1 *Digging with Soil Disturbance*

The simulation results for digging operation in the presence of soil (i.e. uncertain external resistive force on the bucket) is shown in Fig. 9-13. Here, a resistive force on the bucket tip is modeled as a sinusoid of bias $50kN$, $30kN$ combined with random disturbance both into the direction of positive x- and y-axis (see Fig. 10), since resistive force when digging soil is order of $10 \sim 10^2 kN$ for an excavator in similar size with ours, depending only on the geometry of the bucket-terrain intersection and the inherent property of the soil [9]. Note that, this force is only applied when the bucket tip position is lower than the ground level (black dotted line at $y = -1m$ in Fig. 9).

The bucket tip trajectory $(\mathbf{p_b}, \phi_b)$ is shown the Fig. 9, which shows that the control algorithm well follows the desired bucket tip trajectory. The Fig. 11 shows bucket

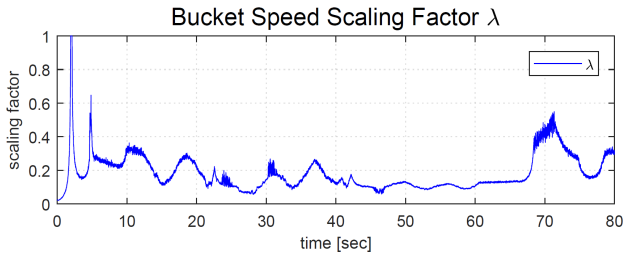

Fig. 11. Bucket speed scaling factor λ obtained by solving the constrained optimization (37) via the divide-and-conquer algorithm Alg. 1 when bucket is moving in the soil disturbance.

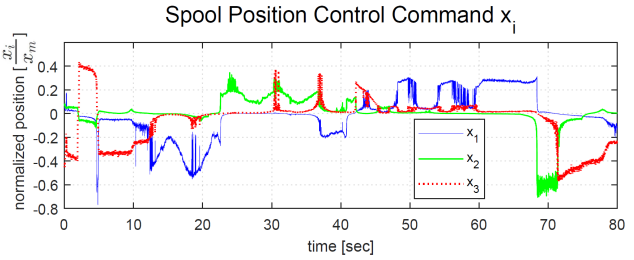

Fig. 12. Spool position control commands x_i, $i = 1, 2, 3$, each for the four-way directional valves of boom (blue), arm (green), and bucket (red) cylinders, calculated from (42) for the scaling factor λ value in Fig. 11 when bucket is moving in the soil disturbance.

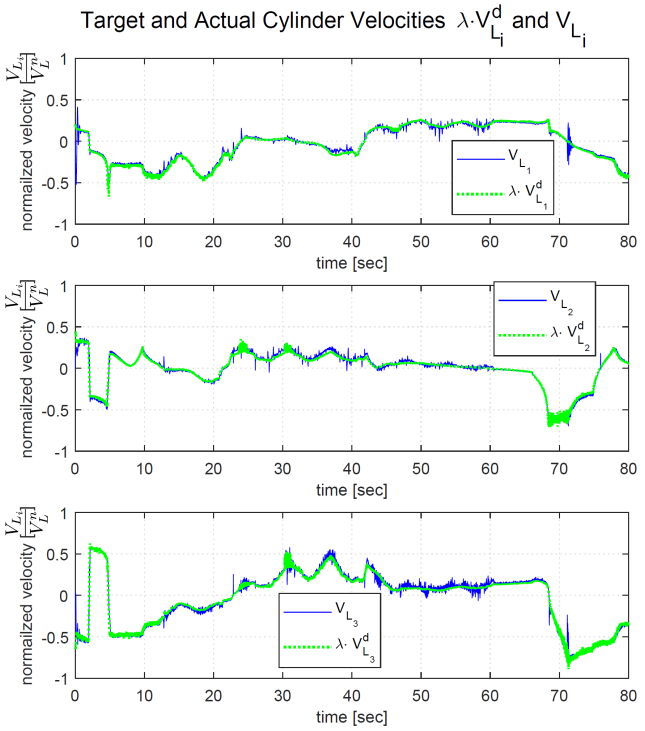

Fig. 13. Scaled target velocities $\lambda V_{L_i}^d$, $i = 1, 2, 3$, (green dotted lines) and actual velocities V_{L_i}, $i = 1, 2, 3$, (blue lines) of the strokes of the boom, arm, and bucket cylinders when bucket is moving in the soil disturbance.

speed scaling factor λ obtained by solving the constrained optimization (37) via the divide-and-conquer algorithm Alg. 1. From the both results, it is shown that the controller follows the desied trajectory by maintaining the direction of the desired bucket tip velocity, while scaling down its speed (i.e. $\lambda < 1$) when the flow saturation occurs due to the inequality constraints (29)-(30), (36), and (13). The scaled target velocities $\lambda V_{L_i}^d$ are shown in Fig. 13, and the corresponding desired control commands x_i, $i = 1, 2, 3$, calculated from (42) are shown in Fig. 12. We can see that the actual velocities of each cylinder V_{L_i}, $i = 1, 2, 3$, simultaneously well tracks the scaled target velocities (see Fig. 13) even though they are still coupled in the MCV. The result Fig. 9 implies our control algorithm is robust against external disturbances owing to the compensation of piston load force $F_{L,i}$ via chamber pressure sensing. This also means that the manipulator inertia/damping, which are typically high, are appropriately compensated in the soil digging.

Note that, velocity may fluctuate due to fluid compliance during the operation particularly when: 1) the soil disturbance containing high-frequency components are applied, or 2) the spool positions crosses $x_i = 0$ (with some deadband) so that the cylinder velocity direction suddenly changes (see Fig. 12). This fast fluctuation of velocity due to fluid compliance and the inertia of the excavator, however, does not affect much the bucket trajectory owing to an averaging effect stemming from the large mechanical inertia and damping, i.e., our steady-state assumption for the valve and cylinder modeling is valid (see Fig. 9).

Fig. 11-13 shows that the speed scaling factor λ and the control input x_i also contains some high-frequency components due to the noise of the chamber pressure measurements $(P_{A,i}, P_{B,i})$ used in the constrained optimization (37). Despite all of the model uncertainties and sensor inaccuracies described above, the maximum error of the path following performance is $4.6cm$. Note that, we omit the simulation results with accurate model parameters and sensors due to the page limit, though it gives an almost perfect control performances.

5.2 Digging with Obstacle

In addition, we simulate the bucket encountered to a hard obstacle during a digging motion along a curved trajectory (see Fig. 14). When the obstacle is encountered, the bucket tip velocity maintains its direction even under the high external payload, while scaling down its speed, and finally stops with $\lambda \to 0$ (see Fig. 15). And when the obstacle is suddenly detached, the bucket tip just well follows the desired curved trajectory owing to the velocity-field control framework. This suggests an enhancement of safety when following some curved trajectories in the presence of hard underground obstacles, as motivated previously in Sec. 2.

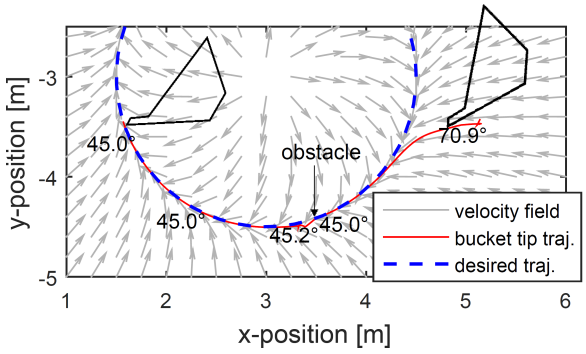

Fig. 14. The bucket tip position $\mathbf{p_b}$ trajectory (red line) and angle w.r.t. ground ϕ_b at every 5 seconds (numbers in degree along the red line) when an obstacle is encountered for a while and then suddenly detached.

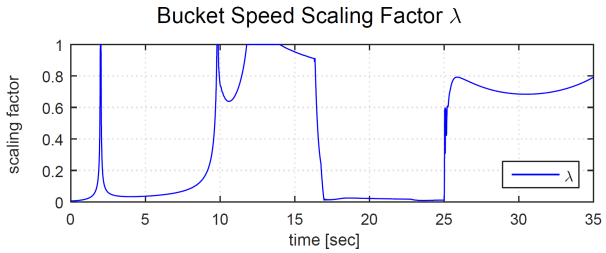

Fig. 15. The bucket tip velocity automatically vanishes (i.e. $\lambda \to 0$) when contacting the hard obstacle, while maintaining its desired bucekt tip velocity direction, and also well operates after the obstacle is suddenly removed.

6 Conclusion

In this paper, we propose a novel control framework for an autonomous excavator with MCV, where the bucket is controlled to follow the direction of the desired velocity-field even under the hydraulic coupling, flow saturation and internal switching in MCV. A constrained-optimization formulation is presented to attain this velocity-field control objective under the physical limitations/constraints of the MCV, which can be solved in real-time by a divide-and-conquer manner with the solution existence/optimality (or local optimality) guaranteed, with each step requiring only to solve two scalar equations via Newton-Raphson method and checking eight explicit scalar inequalities. Simulation results using realistic Simulink/Sim-Hydraulics model show that our proposed control framework properly functions (i.e. well-follows the desired trajectory) with robustness and inherent safety. Some future research topics include: 1) automatic generation of velocity-field to encode representative excavator tasks, 2) design of unified MCV-pump control with the pump control-logic included in the constrained optimization procedure, 3) incorporation of a high-level velocity/path error feedback for better performance/robustness, 4) experiment with a real industrial autonomous excavator, and 5) studies on the more specific operations (e.g. min/max reach) and challenging load conditions.

References

[1] H. Araya and M. Kagoshima. Semi-automatic control system for hydraulic shovel. *Autom. Constr.*, 10:477–486, 2001.

[2] H. Aschemann, T. Meinlschmidt, and H. Sun. An experimental study on decentralised backstepping approaches for a hydrostatic drive train with unknown disturbances. In *Proc. Am. Control Conf.*, pages 874–879, 2014.

[3] B. Bischof, T. Glück, and A. Kugi. Combined path following and compliance control for fully actuated rigid body systems in 3-d space. *IEEE Trans. Control Syst. Technol.*, 25:1750–1760, 2017.

[4] T. Boaventura, J. Buchli, C. Semini, and D. G. Caldwell. Model-based hydraulic impedance control for dynamic robots. *IEEE Trans. Rob.*, 31(6), 2015.

[5] T. Bock. Construction robotics. *Auton. Robot.*, 22:201–209, 2007.

[6] A. Bonchis, P. I. Corke, D. C. Rye, and Q. P. Ha. Variable structure methods in hydraulic servo systems control. *Automatica*, 37(4):589–595, 2001.

[7] E. Budny, M. Chłosta, and W. Gutkowski. Load-independent control of a hydraulic excavator. *Autom. Constr.*, 12(3):245–254, 2003.

[8] H. Cannon. Extended earthmoving with an autonomous excavator. Master's thesis, Robotics Institute, Carnegie Mellon University, 1999.

[9] H. Cannon and S. Singh. Models for automated earthmoving. In *Experimental Robotics VI*, pages 163–172. Springer, London, 2000.

[10] D. Castro-Lacouture. Construction automation. In S. Y. Nof, editor, *Springer Handbook of Automation*, pages 1063–1078. Springer, Berlin, Heidelberg, 2009.

[11] P. H. Chang and S. Lee. A straight-line motion tracking control of hydraulic excavator system. *Mechatronics*, 12:119–138, 2002.

[12] M. G. Doyle. Komatsu launches semi-automatic pc210lci-10 excavator; cuts production time 63%, 2014. `http://www.equipmentworld.com/komatsu-launches-semi-automatic-pc210lci-10-excavator-reduces-production-time-63-by-nixing-over-excavation-photos-video/`.

[13] M. G. Doyle. Caterpillar brings semi-auto grade with assist control to 323f l excavator; grading 45% faster, 2015. `http://www.equipmentworld.com/caterpillar-brings-semi-auto-control-to-323f-l-excavator-new-grade-with-assist-system-makes-grading-45-faster/`.

[14] A. Erdogan, A. C. Satici, and V. Patoglu. Passive velocity field control of a forearm-wrist rehabilitation robot. In *Proc. IEEE Int. Conf. Rehabil. Rob.*, 2011.

[15] D. R. Grandall. The performance and efficiency of hydraulic pumps and motors. Master's thesis, University of Minnesota, 2010.

[16] C. Guan and S. Pan. Nonlinear adaptive robust control of single-rod electro-hydraulic actuator with unknown nonlinear parameters. *IEEE Trans. Control Syst. Technol.*, 16(3):434–445, 2008.

[17] Q. Ha, M. Santos, Q. Nguyen, D. Rye, and H. Durrant-Whyte. Robotic excavation in construction automation. *IEEE Rob. Autom. Mag.*, pages 20–28, 2002.

[18] M. Haga, W. Hiroshi, and K. Fujishima. Digging control system for hydraulic excavator. *Mechatronics*, 11:665–676, 2001.

[19] B. Khoshnevis. Automated construction by contour crafting—related robotics and information technologies. *Autom. Constr.*, 13:5–19, 2004.

[20] J. Koivumäki and J. Mattila. Stability-guaranteed force-sensorless contact force/motion control of heavy-duty hydraulic manipulators. *IEEE Trans. Rob.*, 31(4):918–935, 2015.

[21] M. Krishna and J. Bares. Constructing hydraulic robot models using memory-based learning. *J. Aerosp. Eng.*, 12(2):34–42, 1999.

[22] L. Lapierre and D. Soetanto. Nonlinear path-following control of an auv. *Ocean Eng.*, 34:1734–1744, 2007.

[23] P. Y. Li and R. Horowitz. Passive velocity field control (pvfc): Part ii—application to contour following. *IEEE Trans. Autom. Control*, 46(9):1360–1371, 2001.

[24] P. Y. Li and K. Krishnaswamy. Passive bilateral teleoperation of a hydraulic actuator using an electrohydraulic passive valve. *Int. J. Fluid Power*, 5(2):43–56, 2004.

[25] J. Medanic, M. Yuan, and B. Medanic. Robust multivariable nonlinear control of a two link excavator: Part i. In *Proc. 36th IEEE Conf. Decis. Control*, pages 4231–4236, 1997.

[26] H. E. Merritt. Hydraulic control systems. John Wiley & Sons, New York, 1967.

[27] H. A. Mintsa, R. Venugopal, J.-P. Kenne, and C. Belleau. Feedback linearization-based position control of an electrohydraulic servo system with supply pressure uncertainty. *IEEE Trans. Control Syst. Technol.*, 20(4):1092–1099, 2012.

[28] J. Park, D. Cho, S. Kim, Y. B. Kim, P. Y. Kim, and H. J. Kim. Utilizing online learning based on echo-state networks for the control of a hydraulic excavator. *Mechatronics*, 24(88):986–1000, 2014.

[29] Z. Quan, L. Quan, and J. Zhang. Review of energy efficient direct pump controlled cylinder electro-hydraulic technology. *Renewable Sustainable Energy Rev.*, 35:336–346, 2014.

[30] A. Shenouda. Quasi-static hydraulic control systems and energy savings potential using independent metering four-valve assembly configuration. Master's thesis, Georgia Institute of Technology, 2006.

[31] B. Siciliano. Kinematic control of redundant robot manipulators: A tutorial. *J. Intell. Rob. Syst.*, 3:201–212, 1990.

[32] S. Tafazoli, C. W. de Silva, and P. D. Lawrence. Tracking control of an electrohydraulic manipulator in the presence of friction. *IEEE Trans. Control Syst. Technol.*, 6(3):401–411, 1998.

[33] S. Tafazoli, S. E. Salcudean, K. Hashtrudi-Zaad, and P. D. Lawrence. Impedance control of a teleoperated excavator. *IEEE Trans. Control Syst. Technol.*, 10(3):355–366, 2002.

[34] Trimble Civil Engineering & Construction. Grade control for excavators, 2019. `https://construction.trimble.com/products-and-solutions/grade-control-excavators`.

[35] P. Vähä, T. Heikkilä, P. Kilpeläinen, M. Järviluoma, and E. Gambao. Extending automation of building construction — survey on potential sensor technologies and robotic applications. *Autom. Constr.*, 36:168–178, 2013.

[36] S. Yu, X. Li, H. Chen, and F. Allgöwer. Nonlinear model predictive control for path following problems. In *Proc. 4th IFAC Nonlin. Model Predictive Control Conf.*, pages 145–150, 2012.